Introduction

One thing is certain about this book: by the time you read it, parts of it will be out of date. The study of exoplanets, planets orbiting around stars other than the Sun, is a new and fast-moving field. Important new discoveries are announced on a weekly basis. This is arguably the most exciting and fastest-growing field in astrophysics. Teams of astronomers are competing to be the first to find habitable planets like our own Earth, and are constantly discovering a host of unexpected and amazingly detailed characteristics of the new worlds. Since 1995, when the first exoplanet was discovered orbiting a Sun-like star, over 400 of them have been identified. A comprehensive review of the field of exoplanets is beyond the scope of this book, so we have chosen to focus on the subset of exoplanets that are observed to transit their host star (Figure 1).

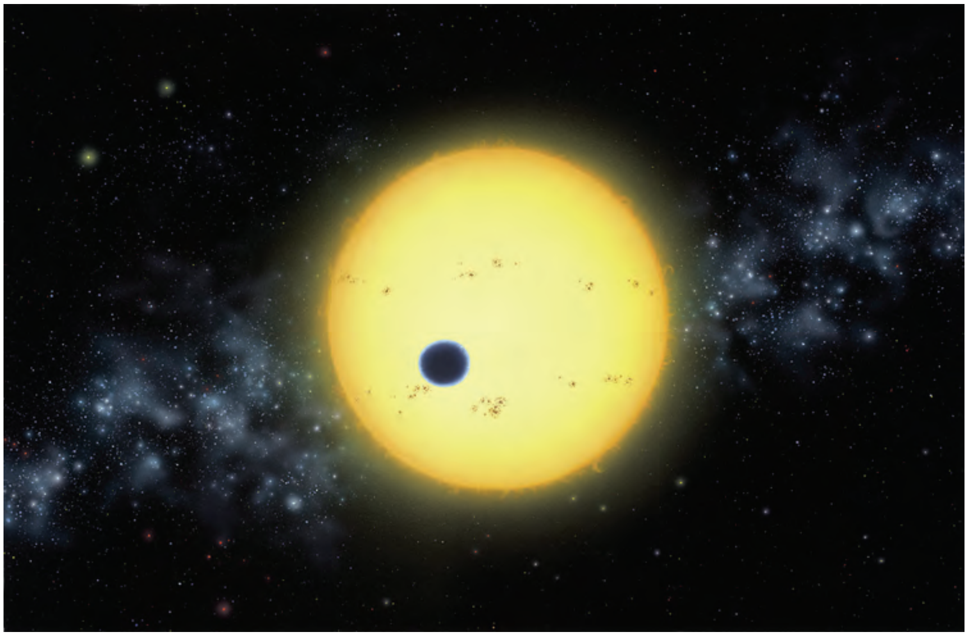

Figure 1 An artist's impression of the transit of HD 209458 b across its star.

These transiting planets are of paramount importance to our understanding of the formation and evolution of planets. During a transit, the apparent brightness of the host star drops by a fraction that is proportional to the area of the planet: thus we can measure the sizes of transiting planets, even though we cannot see the planets themselves. Indeed, the transiting exoplanets are the only planets outside our own Solar System with known sizes. Knowing a planet's size allows its density to be deduced and its bulk composition to be inferred. Furthermore, by performing precise spectroscopic measurements during and out of transit, the atmospheric composition of the planet can be detected. Spectroscopic measurements during transit also reveal information about the orientation of the planet's orbit with respect to the stellar spin. In some cases, light from the transiting planet itself can be detected; since the size of the planet is known, this can be interpreted in terms of an empirical effective temperature for the planet. That we can learn so much about planets that we can't directly see is a triumph of twenty-first century science.

This book is divided into eight chapters, the first of which sets the scene by examining our own solar neighbourhood, and discusses the various methods by which exoplanets are detected using the Solar System planets as test cases. Chapter 2 describes how transiting exoplanets are discovered, and develops the related mathematics. In Chapter 3 we see how the transit light curve is used to derive precise values for the radius of the transiting planet and its orbital inclination. Chapter 4 examines the known exoplanet population in the context of the selection effects inherent in the detection methods used to find them. Chapter 5 discusses the information on the planetary atmosphere and on the stellar spin that can be deduced from spectroscopic studies of exoplanet transits. In Chapter 6 the light from the planet itself is discussed, while in Chapter 7 the dynamics of transiting exoplanets are analyzed. Finally, in Chapter 8 we briefly discuss the prospects for further research in this area, including the prospects for discovering habitable worlds.

The book is designed to be worked through in sequence; some aspects of later chapters build on the knowledge gained in earlier chapters. So, while you could dip in at any point, you will find if you do so that you are often referred back to concepts developed elsewhere in the book. If the book is studied sequentially it provides a self-contained, self-study course in the astrophysics of transiting exoplanets.

A special comment should be made about the exercises in this book. You may be tempted to regard them as optional extras to help you to revise. *Do not fall into this trap!* The exercises are not part of the *revision*, they are part of the *learning*. Several important concepts are developed through the exercises and nowhere else. Therefore you should attempt each of them when you come to it. You will find full solutions for all exercises at the end of this book, but do try to complete an exercise yourself first before looking at the answer. An Appendix containing physical constants is included at the end of the book; use these values as appropriate in your calculations.

For most calculations presented here, use of a scientific calculator is essential. In some cases, you will be able to work out order of magnitude estimates without the use of a calculator, and such estimates are invariably useful to check whether an expression is correct. In some calculations you may find that use of a computer spreadsheet, or graphing calculator, provides a convenient means of visualizing a particular function. If you have access to such tools, please feel free to use them.

Chapter 1 Our Solar System from afar

Introduction

In 1972 a NASA spacecraft called Pioneer 10 was launched. It is the fastest-moving human artefact to have left the Earth: 11 hours after launch it was further away than the Moon. In late 1973 it passed Jupiter, taking the first close-up images of the largest planet in our Solar System. For 25 years Pioneer 10 transmitted observations of the far reaches of our Solar System back to Earth, passing Pluto in 1983 (Figure 1.1).

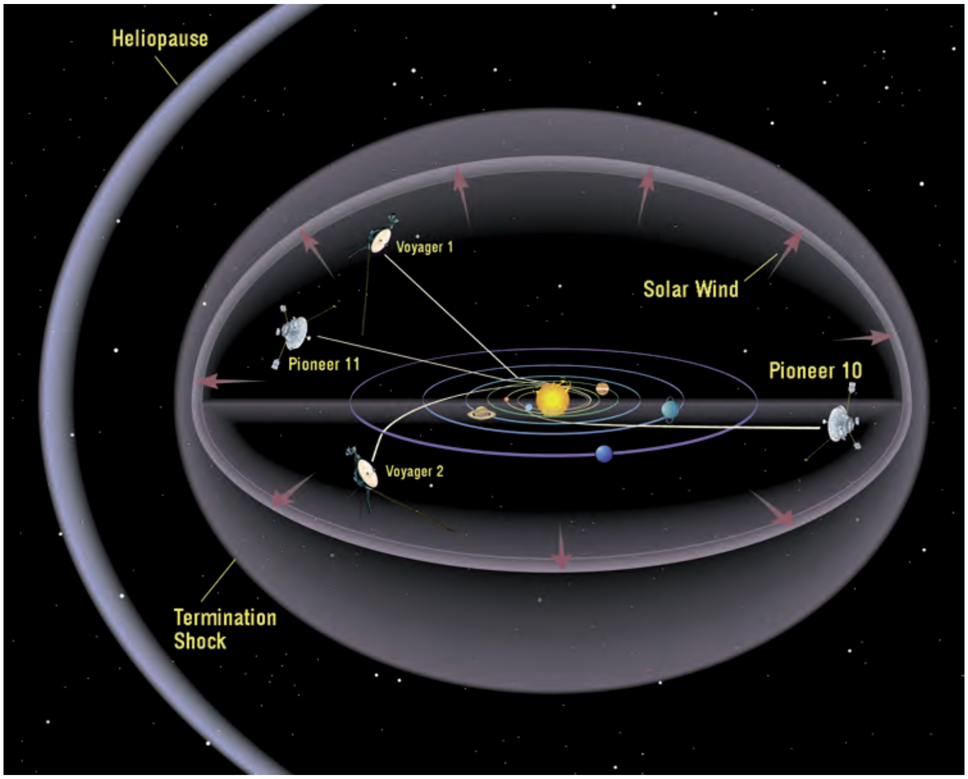

Figure 1.1 The trajectories of Pioneer 10 and other space probes. The heliopause is the boundary between the heliosphere, which is dominated by the solar wind, and interstellar space. The solar wind is initially supersonic and becomes subsonic at the termination shock. Note: all objects are *much* smaller than they have been drawn!

At final radio contact, it was 82 AU (or equivalently 1.2×10^{13} m) from the Sun. It continues to coast silently towards the red star Aldebaran in the constellation Taurus. It is 68 light-years to Aldebaran, and it will take Pioneer 10 two million years to cover this distance. During this time, of course, Aldebaran will have moved.

Any single star may have several different names. This is especially true of bright stars, e.g. Aldebaran is also known as α Tau. We have generally tried to adopt the names most frequently used in the exoplanet literature.

Figures 1.2 and 1.3 show the Sun's place in our Galaxy. The 10-light-year scale-bar in Figure 1.2a is 2000 times the radius of Neptune's orbit: Neptune is the furthest planet from the Sun shown in Figure 1.1. The structure of our own Solar System shown in Figure 1.1 is invisibly tiny on the scale of Figure 1.2a. To render them visible, all the stars in Figure 1.2a are shown larger than they really are. Interstellar space is sparsely populated by stars. The successive parts of Figures 1.2 and 1.3 zoom out from the view of our immediate neighbourhood. In Figure 1.2b we see a more or less random pattern of stars, which includes the Hyades cluster and the bright stars in Ursa Major. All the stars shown in Figure 1.2b belong to our local spiral arm, which is called the Orion Arm.

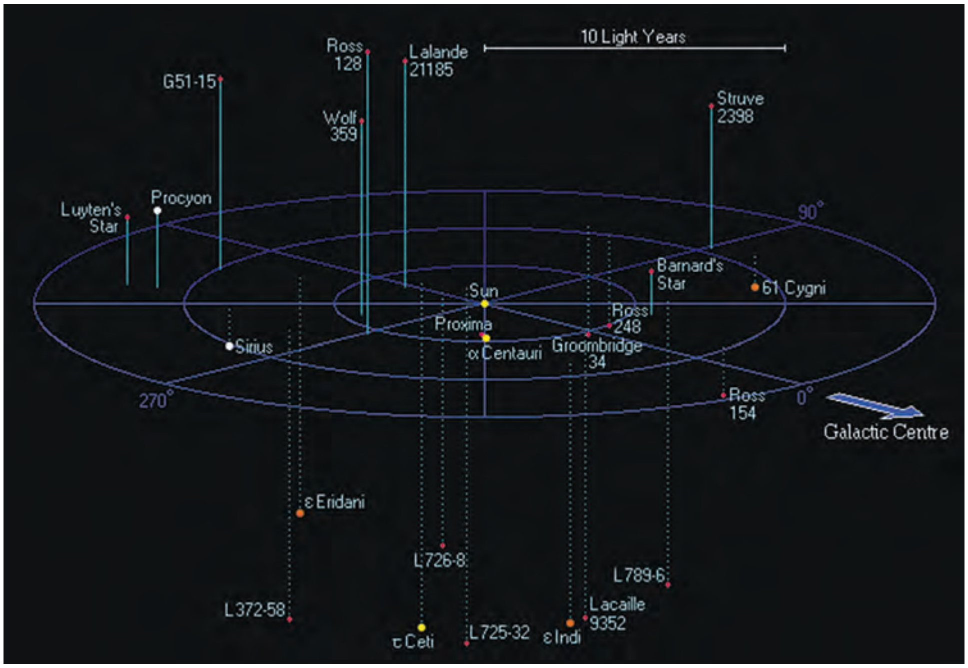

(a)

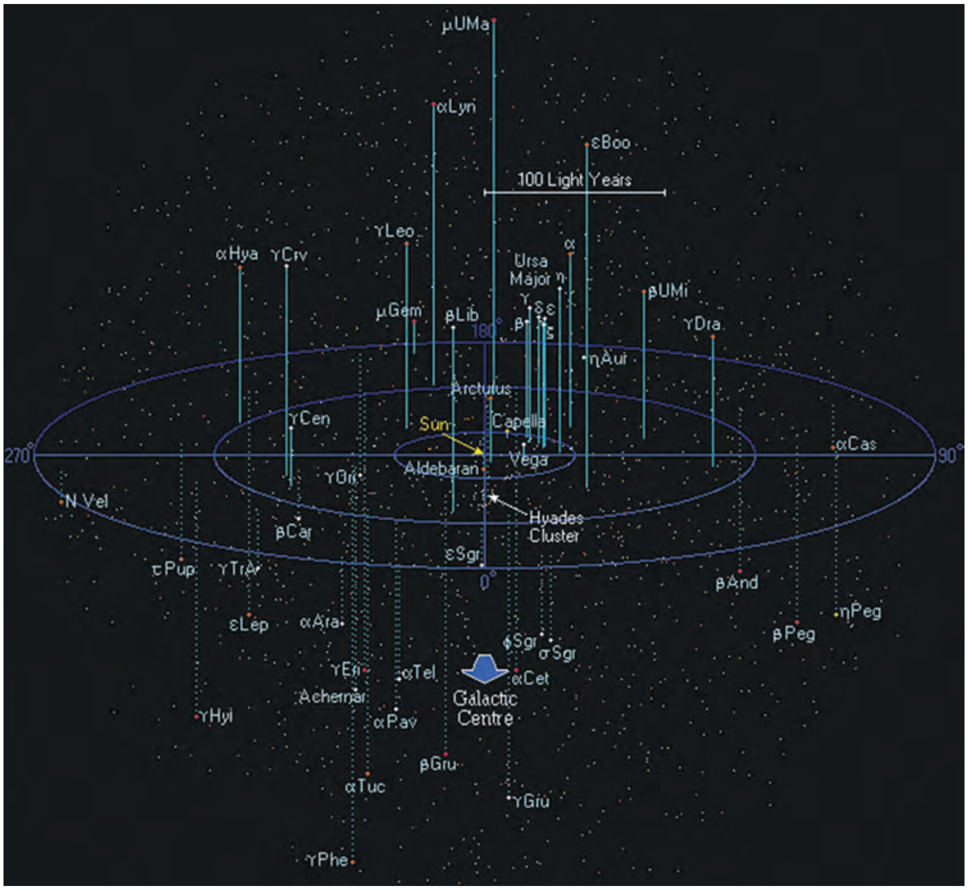

(b)

Figure 1.2 (a) The stars within 12.5 light-years of the Sun. (b) The solar neighbourhood within 250 light-years.

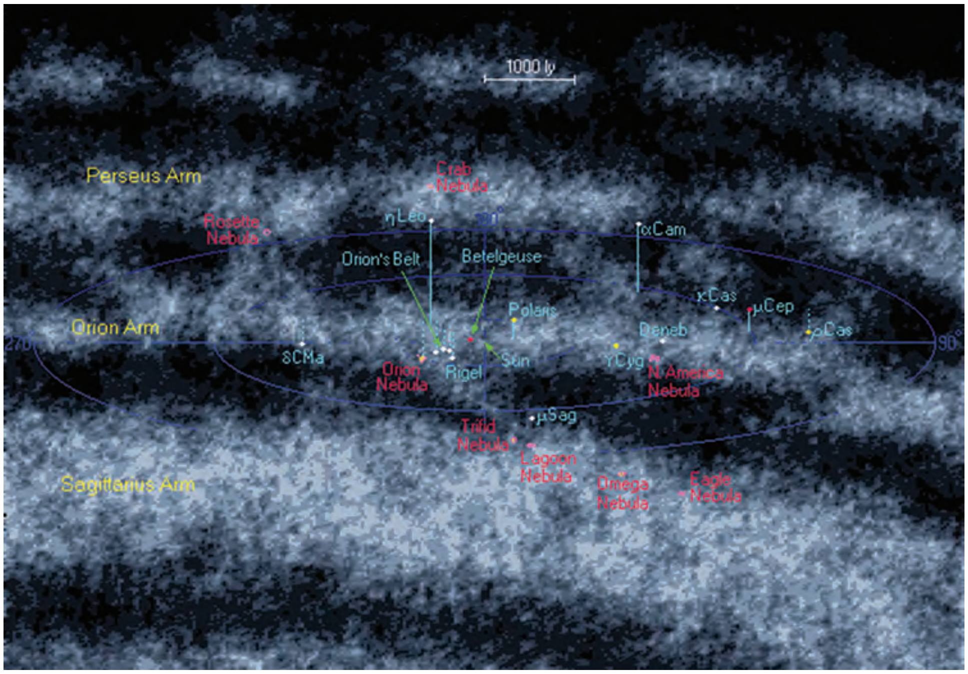

(a)

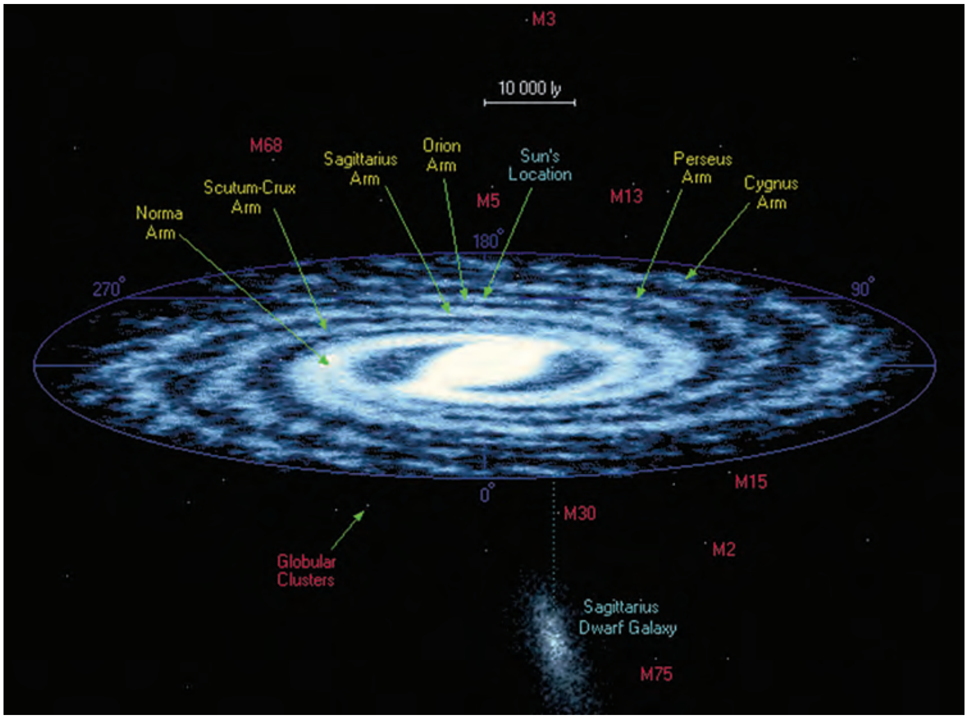

(b)

Figure 1.3 (a) Our part of the Orion Arm and the neighbouring arms. (b) Our Milky Way Galaxy.

Figure 1.3a shows our sector of the Galaxy: a view centred on the Sun, which is a nondescript star lost in the host of stars comprising the Orion Arm. The bright stars of Orion, familiar to many people from the naked-eye night sky, are prominent in this view: they give our local spiral arm its name. Finally, Figure 1.3b shows our entire Galaxy.

Exercise 1.1 Pioneer 10 is coasting through interstellar space at a speed of approximately 12 km s^{-1}. Confirm the time that it will take to cover the 68 light-years to Aldebaran's present position. *Hint*: The Appendix gives conversion factors between units. ■

Confusingly, the standard symbol for astronomical parallax is π, which is more frequently used as the symbol for the constant relating the diameter and circumference of a circle. Usually it is easy to work out which meaning is intended.

The nearest stars and planets

Planets have been detected around 6 of the 100 nearest stars (October 2009), including the Sun. Throughout this book, where new results are frequent, we indicate in parentheses the date at which a statement was made, as we did in the previous sentence. Table 1.1 lists the seven known planetary systems within 8 pc.

Table 1.1 Stars within 8 pc with known planets. (In accordance with the IAU we list 8 planets in the Solar System; we will not comment further on the status of Pluto and similar dwarf planets.)

Name (alias)	Parallax, π/arcsec	Spectral type	V	M_V	Mass ($M_\odot$)	Known planets
Sun	—	G2V	−26.72	4.85	1.00	8
ε Eri (GJ 144)	0.309 99 ±0.00079	K2V	3.73	6.19	0.85	1
GJ 674	0.220 25 ±0.00159	M3.0V	9.38	11.09	0.36	1
GJ 876 (IL Aqr)	0.212 59 ±0.00196	M3.5V	10.17	11.81	0.27	3
GJ 832 (HD 204961)	0.202 52 ±0.00196	M1.5V	8.66	10.19	0.45	1
GJ 581 (HO Lib)	0.159 29 ±0.00210	M2.5V	10.56	11.57	0.30	3
Fomalhaut (αPsA/GJ881)	0.130 08 ±0.00092	A3V	1.16	1.73	2.1	1

These data were taken from the information on the 100 nearest stars on the Research Consortium on Nearby Stars (RECONS) website, which is updated annually. Fomalhaut, which is nearby, but not one of the 100 nearest stars, was added because the planet Fomalhaut b was recently discovered, as we will see in Subsection 1.1.1. Table 1.1 gives the values of the parallax, π, the spectral type, the apparent V band magnitude, V, and the absolute V band magnitude, M_V, as well as the stellar mass and the number of known planets. It is very noticeable that over half of these nearby planet host stars are M dwarfs, the lowest-mass, dimmest and slowest-evolving main sequence stars. By the time you read this, more nearby planets will probably have been discovered.

The nearest stars have distances directly determined by geometry using trigonometric parallax, and the RECONS sample (Figure 1.4) includes 249 systems within 10 pc, or equivalently 32.6 light-years, all with distances known to 10% or better. 72% of the stars are M dwarfs. M dwarfs are the faintest main sequence stars, so although they predominate in the solar neighbourhood, they are more difficult to detect than other more luminous stars, particularly at large distances.

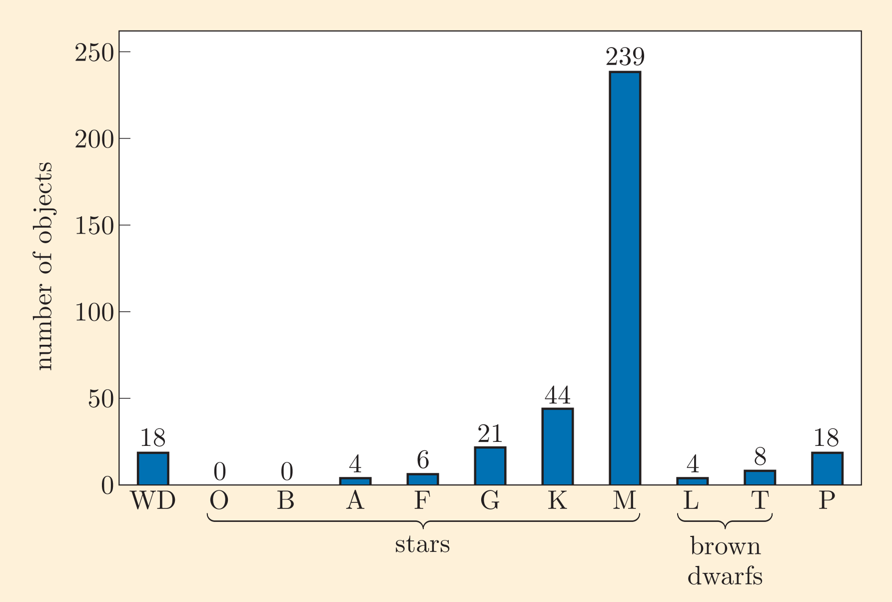

Figure 1.4 Known objects within 10 parsecs (RECONS 2008). The leftmost column shows white dwarfs, columns 2–8 show stars subdivided by spectral type, columns 9 and 10 show L and T class brown dwarfs, and the last column shows known planets, including eight in our own Solar System. The stars in the census are overwhelmingly M dwarf stars, i.e. low-mass main sequence stars.

The census illustrated in Figure 1.4 is likely to be more representative of stellar demographics than a sample limited by apparent brightness would be. The numbers in this census include the Sun and its eight planets. The 362 objects represented in Figure 1.4 are comprised of 170 systems containing a single object, 58 double systems (either binary stars or star plus single planet systems), and 21 multiple systems, including our own Solar System. New objects are being discovered continually, and this census grew by 20% between January 2000 and January 2008.

While not quite close enough to be included in Table 1.1, or in the census illustrated in Figure 1.4, HD 160691 at a distance of 15.3 pc deserves a mention: it has 4 known planets. The recently discovered planet GJ 832 b is a giant planet with an orbital period between 9 and 10 years: i.e. it has pronounced similarities to the giant planets in our own Solar System. GJ 832 b has mass $M_\mathrm{P} = 0.64 \pm 0.06\,\mathrm{M_J}$, where $\mathrm{M_J}$ is the mass of Jupiter, i.e. $1898.13 \pm 0.19 \times 10^{24}$ kg. The properties of its host star, GJ 832, are given in Table 1.1.

- With reference to Table 1.1, what is the distance to the nearest known exoplanetary system?

- ε Eri (GJ 144) has the largest parallax of all known exoplanetary systems, with $\pi = 0.309\,99 \pm 0.000\,79$ arcsec. The distance, d, in parsecs is given by

$$\frac{d}{\text{pc}} = \frac{1}{\pi/\text{arcsec}},$$

so the distance to ε Eri is $0.309\,99^{-1}$ pc, or 3.226 pc. The uncertainty on the parallax measurement is 0.25%, so the uncertainty in the distance determination is approximately 0.25% of 3.226 pc. Hence, to four significant figures, the distance to the nearest known exoplanetary system is 3.226 ± 0.008 pc. Converting this to SI units, 1 pc is 3.086×10^{16} m, so the distance to GJ 144 is $(9.96 \pm 0.02) \times 10^{16}$ m.

As you can see in Figure 1.2b, Aldebaran is actually an extremely nearby star when we consider our place in the Milky Way Galaxy, so the example of Pioneer 10's journey shows just how distant the stars are, compared to the interplanetary distances in our own Solar System. Until 1995, we knew of no planets orbiting around other stars similar to our own Sun. Given the distances involved, and the extreme dimness of planets compared to main sequence stars, this is hardly surprising.

Stars, planets and brown dwarfs

This book will primarily discuss giant planets and their host stars. Objects with masses too small to ignite hydrogen burning in their cores, yet massive enough to have fused deuterium, are known as **brown dwarfs**. This implies that brown dwarfs have masses less than about $80\,M_J$. While there is no universally agreed definition, giant planets are often defined as objects that are less massive than brown dwarfs and have failed to ignite deuterium burning. Adopting this definition, planets have masses less than about $13\,M_J$. Stars, brown dwarfs and giant planets form a sequence of declining mass.

Figure 1.5a compares two examples of main sequence stars with two brown dwarfs, one old and one young, and giant planets with masses of $1\,M_J$ and $10\,M_J$. It is clear that the brown dwarfs and giant planets are all roughly the same size, while the Sun and the MV star Gliese 229A differ radically in size and effective temperature, despite having masses of the same order of magnitude. These most basic characteristics arise because of the physics operating to support these various objects against self-gravity, some of which we will explore in Chapter 4 of this book. When discussing exoplanets, astronomers use the mass of Jupiter, M_J, or the mass of the Earth, $M_\oplus$, as a convenient mass unit, just as the mass of the Sun is used as a convenient unit in discussing stars. The values of these units are given in the Appendix. (Table 4.1 in Chapter 4 gives conversion factors between the units.)

Figure 1.5b shows part of the Sun and the Solar System planets, immediately revealing the huge difference in size between the giant planets and the terrestrial planets. It is because giant planets are so much bigger than terrestrial planets that almost all the transiting exoplanets discovered so far (Dec.2009) are giant planets. As we will see in Chapter 4, giant planets are

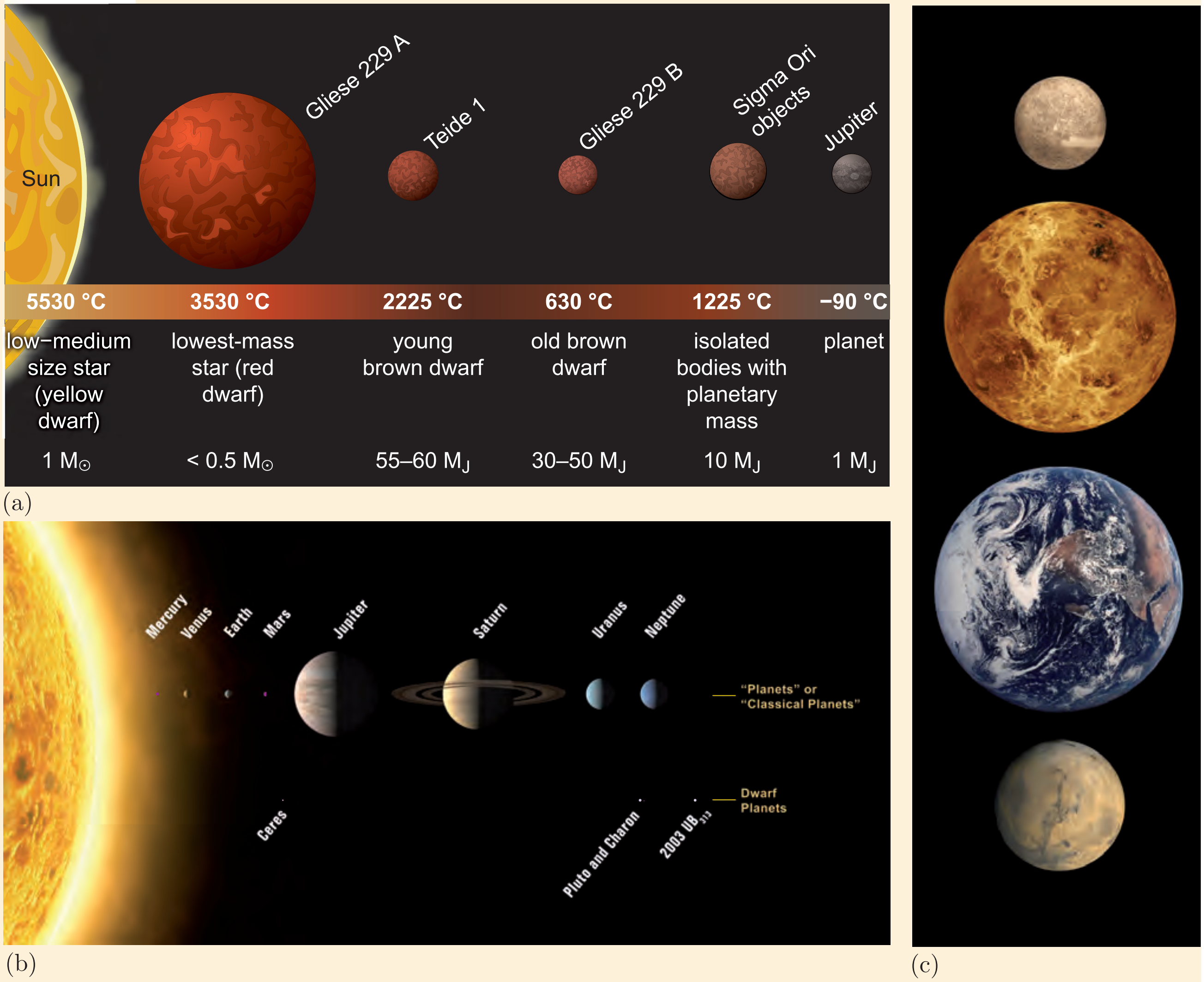

Figure 1.5 Comparisons of stars, brown dwarfs and planets. (a) Two main sequence stars, two brown dwarfs, and two objects of planetary mass, arranged in a sequence of declining mass. Neither the radius nor the surface temperature follows the mass sequence exactly. (b) The Sun and its planets. The giant planets are much larger than the terrestrial planets. (c) The Solar System's terrestrial planets in order of distance from the Sun: Mercury, Venus, Earth and Mars, from top to bottom.

formed predominantly of gas or ice, i.e. low-density material. The terrestrial planets, as we know from our intimate experience of the Earth, have solid surfaces composed of rock, and are denser than giant planets by about a factor of three. Jupiter is over 300 times more massive than the Earth, and has a radius about 10 times bigger, i.e. a volume 1000 times bigger. Generally, terrestrial planets are thought to have lower mass than giant planets: this is certainly true in the Solar System. There may, however, be **mini-Neptune** ice giant exoplanets with lower masses than **super-Earth** terrestrial exoplanets. Since few transiting exoplanets with masses below $10\,M_\oplus$ are yet known (Dec. 2009), this remains an open question, though one that we will explore later.

Could extraterrestrial astronomers detect the Solar System planets?

So far, in this Introduction and in the boxes entitled 'The nearest stars and planets' and 'Stars, planets and brown dwarfs', we have set our own Solar System in the context of its place in our Milky Way Galaxy, and briefly compared **main sequence stars** with brown dwarfs and planets. The subject of the *book* is transiting exoplanets, but to interpret our findings about exoplanets, we need first to understand the various methods that have been or could be used to find them. To this end, in the remainder of this chapter we will use the familiar Solar System planets to illustrate the various exoplanet detection methods. We will examine the question: *If the Galaxy harbours intelligent life outside our own Solar System, could these hypothetical extraterrestrials detect the Solar System planets?* Each of the exoplanet detection methods will be applied to the Solar System, and through this the limitations for each method will be explored.

1.1 Direct imaging

The Solar System planets were all, of course, detected from Earth using direct imaging (Figure 1.6). Obviously, direct imaging works best for nearby objects, and becomes more difficult as the distance, d, to an object increases, as Figure 1.7 demonstrates.

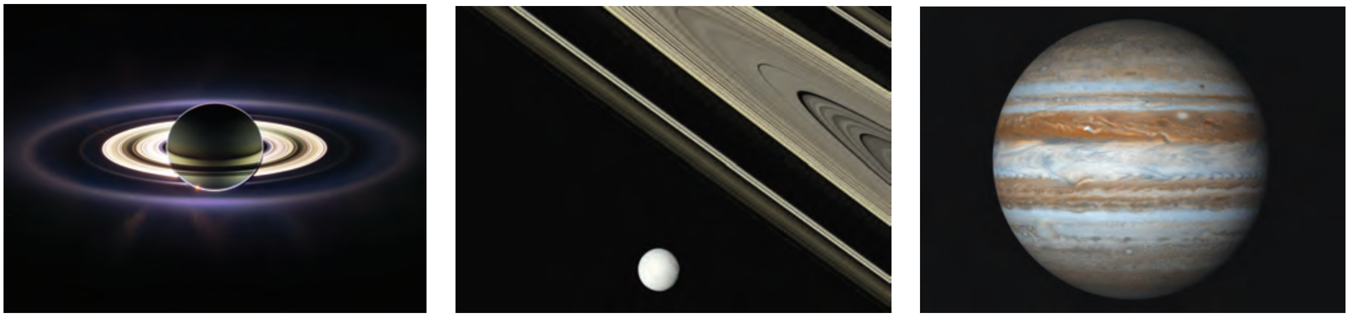

(a) (b) (c)

Figure 1.6 NASA images of Saturn and Jupiter. (a) The back-lit rings of Saturn observed by Cassini. (b) Saturn's moon Tethys and a close-up of the rings. (c) Jupiter, the largest planet in the Solar System.

This is particularly true if the object to be imaged is close to a brighter object. Since the optical light from the Solar System's planets is overwhelmingly reflected sunlight, this is clearly the case for them. The biggest and most luminous planet in the Solar System, Jupiter, reflects about 70% of the sunlight that it intercepts, and consequently has a luminosity of $\sim 10^{-9}\,L_\odot$.

- Compare the position of Voyager 1 when the images in Figure 1.7 were taken, with the distance to the nearest known exoplanetary system. How many times further away is the nearest known exoplanet?

- Voyager 1 was 6.4×10^{12} m from the Earth, while the distance to the nearest known exoplanetary system, ε Eri, is $9.96 \pm 0.02 \times 10^{16}$ m. The ratio of these two distances is 15 560: the nearest known exoplanetary system is over 15 000 times further away.

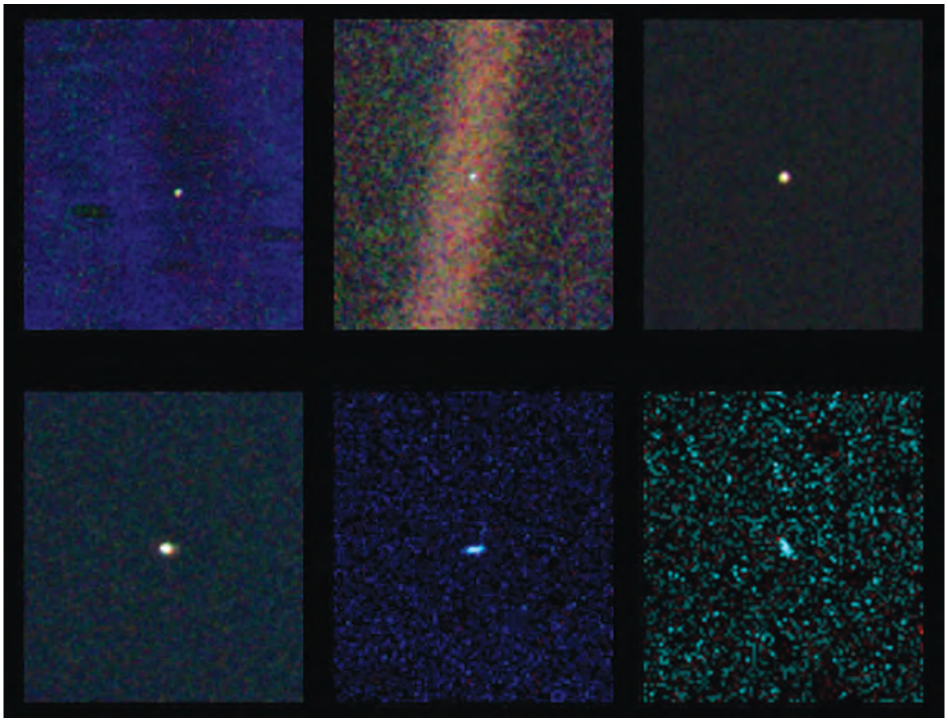

Figure 1.7 These images show six of the Solar System's planets. They were taken by Voyager 1 from a position similar to where it is shown in Figure 1.1, more than 6.4×10^{12} m from Earth and about 32 degrees above the **ecliptic plane**. Mercury was too close to the Sun to be seen; Mars was not detectable by the Voyager cameras due to scattered sunlight in the optics. Top row, left to right, are Venus, Earth and Jupiter; the bottom row shows Saturn, Uranus and Neptune. The background features in the images are artefacts resulting from the magnification. Jupiter and Saturn were resolved by the camera, but Uranus and Neptune appear larger than they should because of spacecraft motion during the 15 s exposure. Earth appears in the centre of the scattered light rays resulting from the Sun. Earth was a crescent only 0.12 pixels in size. Venus was 0.11 pixels in diameter.

Jupiter is a prominent object in our own night sky, but viewed from ε Eri it is very close to the Sun, which outshines it by a factor of 10^9. Jupiter's **orbital semi-major axis**, a_J, is 7.784×10^{11} m. Using the **small angle formula**, the **angular separation** between the Sun and Jupiter as viewed at the distance of ε Eri is

$$
\begin{aligned}
\theta &= \frac{a_J}{d_{\varepsilon\,\mathrm{Eri}}}\ \text{radians} \\
&= \frac{7.784 \times 10^{11}\,\mathrm{m}}{9.96 \times 10^{16}\,\mathrm{m}}\ \text{rad} \\
&= 7.815 \times 10^{-6}\ \text{rad} \\
&= 7.815 \times 10^{-6} \times \frac{360 \times 60 \times 60}{2\pi}\ \text{arcsec} \\
&= 1.61\ \text{arcsec}.
\end{aligned}
$$

- Does the angular separation of Jupiter and the Sun at the distance of ε Eri depend on the direction from which the Solar System is viewed?

- Yes. The angular separation calculated above is the maximum value, which would be attained only if the system were viewed from above so that the plane of Jupiter's orbit coincides with the **plane of the sky**. Even for edge-on systems, though, the full separation can be observed at two positions on the orbit.

Thus detecting Jupiter from the distance of ε Eri by direct imaging would be extremely challenging, as there is an object $\sim 10^9$ times brighter within 2 arcsec. If Jupiter were brighter and the Sun were fainter this would help, and one way to achieve this is to observe in the infrared. At these wavelengths Jupiter's thermal emission peaks but the Sun's emission peaks at much shorter wavelengths, so the contrast ratio between the Sun and Jupiter is less extreme. Figure 1.8 shows the **spectral energy distributions** of the Sun and four of the Solar System planets as they would be observed at a distance of 10 pc. This figure shows that the contrast ratio between the Sun and the planets becomes generally more favourable at longer wavelengths.

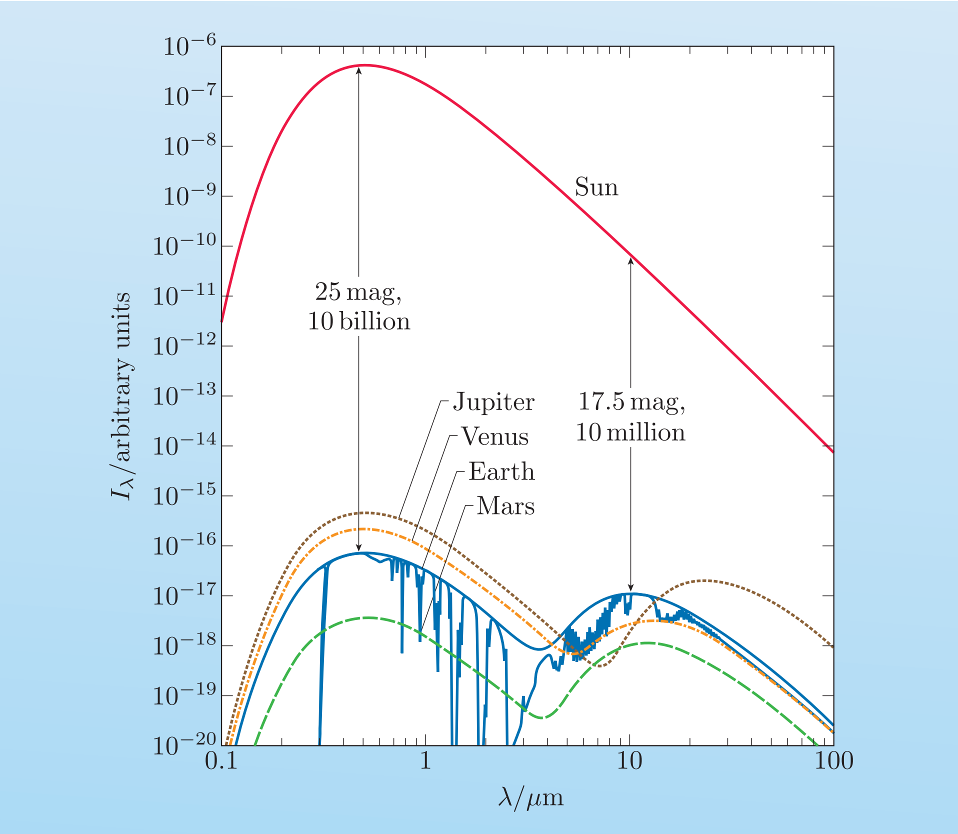

Figure 1.8 The spectral energy distributions of the Sun, Jupiter, Mars, Earth and Venus. The curve for the Earth is far more detailed than the curves for the other objects because empirical data have been included. For each of the planets, the spectral energy distribution is composed of two broad components: peaking at around 0.5 μm is the reflected solar spectrum, while the thermal emission of the planet itself peaks at 9–20 μm.

- Jupiter is the biggest planet in the Solar System, yet at wavelengths around $10\,\mu$m the Earth emits more light. Why is this?

- The Earth is closer to the Sun, and consequently it receives more **insolation**, i.e. more sunlight falls per unit surface area. Thus the Earth is heated to a higher temperature than Jupiter, and the Earth's thermal emission peaks at around $10\,\mu$m. The amount of light emitted is the surface area multiplied by the flux per unit area. The latter depends strongly on temperature, thus the Earth is brighter at $10\,\mu$m despite having approximately 100 times less emitting area.

Planets can have internal sources of energy in addition to the insolation that they receive; for example, radioactive decay of unstable elements generates energy within the Earth. Radioactive decay is generally thought to be insignificant in giant planets as their composition is predominantly H and He. More important for the planets that we will discuss in this book is internal heating generated by gravitational contraction, which is known as **Kelvin–Helmholtz contraction**. Jupiter emits almost twice as much heat as it absorbs from the Sun, and all four giant planets in the Solar System radiate some power generated by Kelvin–Helmholtz contraction.

Exercise 1.2 Figure 1.8 shows the spectral energy distributions for the Sun and four of our Solar System's planets. Consider the following with reference to this figure.

(a) State what wavelength gives the most favourable contrast ratio with the Sun for the detection of Jupiter. What is the approximate value of this most favourable contrast ratio?

(b) At what wavelength does the spectral energy distribution of Jupiter peak? Is this the same wavelength as you stated in part (a)? Explain your answer.

(c) What advantages are there to using a wavelength of around $20\,\mu$m for direct imaging observations of Jupiter from interstellar distances? ■

In fact, infrared imaging has detected an exoplanet directly. A giant exoplanet was discovered at an angular distance of 0.78 arcsec from the brown dwarf 2MASSWJ 1207334-393254 by infrared imaging, as shown in Figure 1.9. Direct imaging is most effective for bright planets in distant orbits around nearby faint stars. These requirements mean that direct imaging has limited applicability in the search for exoplanets. Returning to our hypothetical extraterrestrial astronomers, even if they were located on one of the nearest known exoplanets, they would face problems in detecting even the most favourable of the Solar System's planets by direct imaging. The angular separation of Jupiter from the Sun is less than 2 arcsec, and the Sun is one of the brighter stars in the solar neighbourhood, with the contrast ratio between the Sun and Jupiter being over 10^4 even at the most favourable wavelength. Thus it seems unlikely that hypothetical extraterrestrials would first detect the Solar System planets through direct imaging.

Despite the difficulties, astronomers are designing instruments specifically to detect exoplanets by direct imaging. These instruments employ sophisticated techniques to overcome the overwhelming light from the planets' host stars. The Gemini Planet Imager (GPI) is designed to detect planets with contrast ratios as

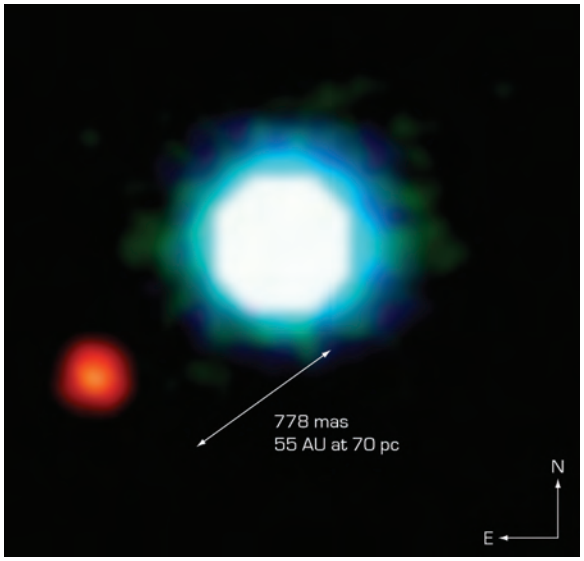

Figure 1.9 False-colour image of the brown dwarf 2MASSWJ 1207334-393254 using H, K and L band infrared filters. Blue indicates pixels brightest in H, while red indicates pixels brightest in L. The companion exoplanet is relatively bright in the L band and thus appears red. The exoplanet has an effective temperature of 1250 ± 200 K.

extreme as 10^8 using a device called a **coronagraph**. A spectacular recent result using this method is summarized in Subsection 1.1.1 below. As Figure 1.8 shows, this technology could in principle render the Earth detectable. In practice, to detect the Earth, the extraterrestrials' telescope would need to be implausibly close to the Solar System.

- If the contrast ratio of the Earth and the Sun is less than the threshold for planet detection with the GPI, what limits the detectability of the Earth with such an instrument at large distances?

- There are two limiting factors. First, the angular separation of the Earth and the Sun decreases with distance; at large distances the two objects are not spatially resolved. The angular separation diminishes as $1/d$. Second, the telescope needs to have sufficient Earthlight falling on it to permit detection of the Earth. The number of photons reaching the telescope diminishes as $1/d^2$.

The SPHERE instrument is scheduled to be deployed on the Very Large Telescope (VLT) in 2010, and aims to detect some nearby young giant exoplanets at large separations from their host star. Giant planets are brightest early in their life, when they are contracting relatively quickly. The Kelvin–Helmholtz powered luminosity diminishes as a giant planet contracts and cools with age, as we will see in Subsection 4.4.3.

1.1.1 Coronagraphy

As the name implies, coronagraphs were invented to study the solar corona by blocking the light from the disc (i.e. the photosphere) of the Sun. An occulting element is included within the instrument, and is used to block the bright object, allowing fainter features to be detected. If an exoplanetary system is close enough for the star and exoplanet to be resolved, then a coronagraph may permit detection of an exoplanet where without it the detector would be flooded with light from the central star.

Fomalhaut (α PsA) is one of the 20 brightest stars in the sky; some of its characteristics were listed in Table 1.1. It is surrounded by a dust disc that appears elliptical and has a sharp inner edge. This led to speculation that there might be a planet orbiting Fomalhaut just inside the dust ring, and creating the sharp inner edge of the ring rather as the moons of Saturn shepherd its rings (cf. Figure 1.6). Figure 1.10 was created using the Hubble Space Telescope's coronagraph, combining two images taken in 2004 and 2006. In this figure the orbital motion of the planet Fomalhaut b is clearly revealed. Fomalhaut b is $\sim 10^9$ times fainter than Fomalhaut, and is ~ 100 AU from the central star.

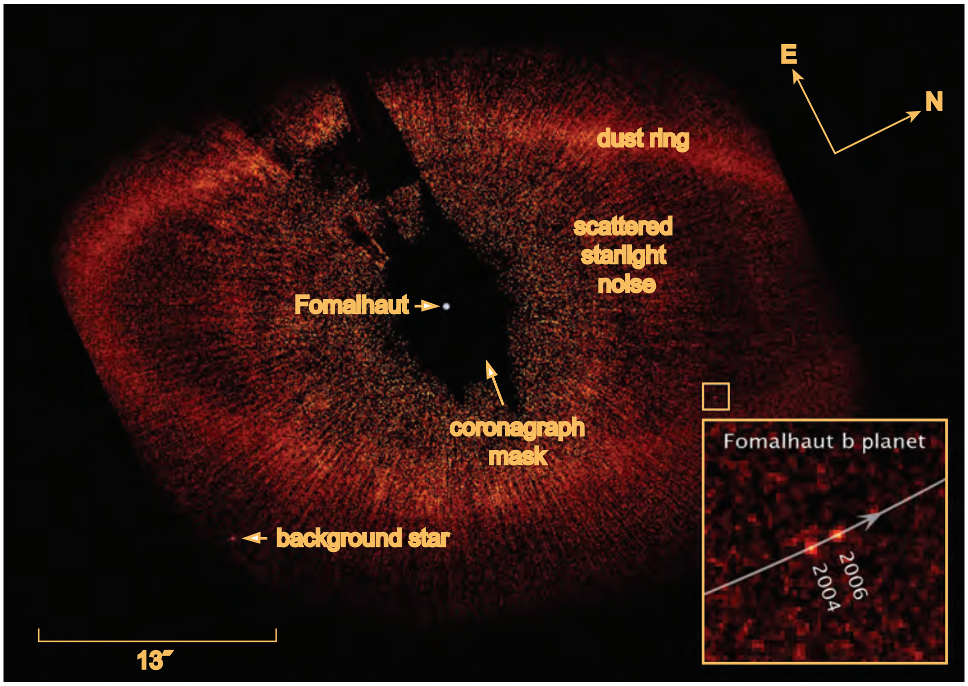

Figure 1.10 False-colour image showing the region surrounding Fomalhaut. The black shape protruding downwards from 11 o'clock is the coronagraph mask, which has been used to block the light from the star located as indicated at the centre of the image. The square box is the region surrounding the planet, which has been blown up and inset. The motion of the planet, called Fomalhaut b, along its elliptical orbit between 2004 and 2006 is clearly seen. At the distance of Fomalhaut 13″ corresponds to 100 AU.

There are designs (though not necessarily the funding) for a space telescope with a coronagraph optimized to detect terrestrial exoplanets: Fomalhaut b may be the first of a significant number of exoplanets detected in this way. Our hypothetical extraterrestrial astronomers could possibly detect the Solar System's planets using coronagraphy, provided that they are close enough to the Sun to be able to block its light without also obscuring the locations of the Sun's planets.

1.1.2 Angular difference imaging

Another spectacular recent result, shown in Figure 1.11, uses some other clever techniques to overcome the adverse planet to star contrast ratio. Figure 1.11 reveals three giant planets around the A5V star HR 8799. The technique employed is called angular difference imaging, an optimal way of combining many short exposures to reveal faint features. HR 8799's age is between 30 Myr and 160 Myr, i.e. it is a young star. Because this planetary system is young, the giant planets are relatively bright, making their detection by direct imaging possible. The three

Myr indicates 10^6 yr, or a megayear.

planets have angular separations of 0.63, 0.95 and 1.73 arcsec from the central star, corresponding to projected separations of 24, 38 and 68 AU. The orbital motion, counter-clockwise in Figure 1.11, was detected by comparing images taken in 2004, 2007 and 2008. The masses of these three bodies are estimated to be between $5\,M_J$ and $13\,M_J$.

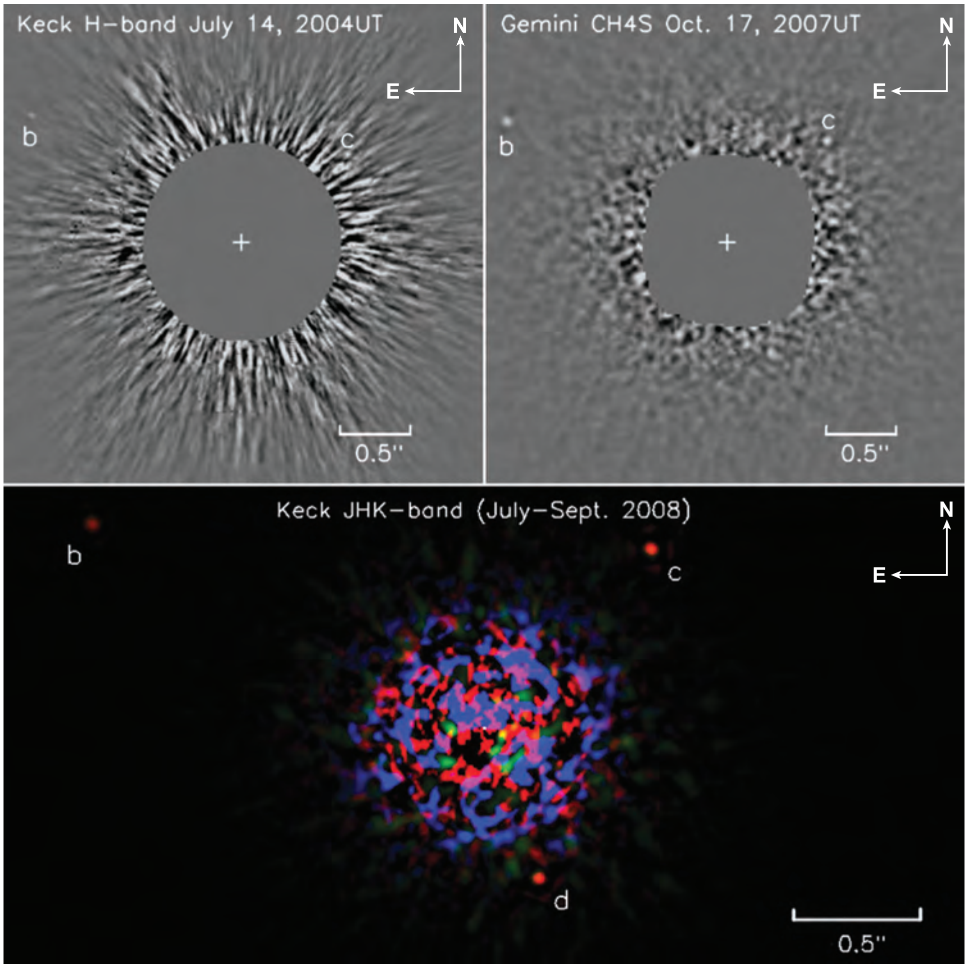

Figure 1.11 The three planets around HR 8799. The central star is overwhelmingly bright and has been digitally removed from the images, causing the featureless or mottled round central region in each panel. The three planets, whose names are HR 8799 b, c and d, are labelled b, c and d. At the distance of HR 8799, 0.5″ corresponds to 20 AU.

1.2 Astrometry

Hipparcos was an ESA satellite that operated between 1989 and 1993.

Astrometry is the science of accurately measuring the positions of stars. The Hipparcos satellite measured the positions of over 100 000 stars to a precision of 1 milliarcsec, and the Gaia satellite, due for launch by the European Space Agency (ESA) in spring 2012, will measure positions to a precision of 10 microarcsec (μarcsec). Astrometry offers a way to indirectly detect the presence of planets. Though we often casually refer to planets orbiting around stars, in fact planets and stars both possess mass, and consequently all the bodies in a planetary system orbit around the **barycentre**, or common centre of mass of the system. Figure 1.12 illustrates this.

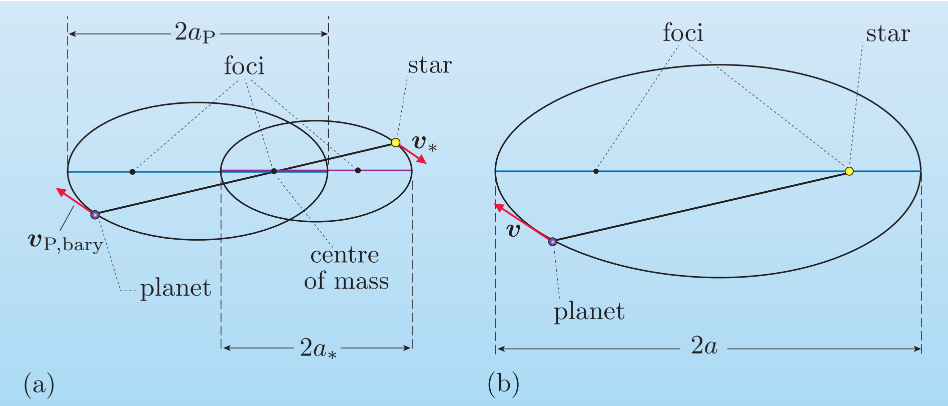

Figure 1.12 (a) The elliptical orbits of a planet and its host star about the barycentre (or centre of mass) of the system. (b) In astrocentric coordinates, i.e. coordinates centred on the star, the planet executes an elliptical orbit with the star at one focus. The semi-major axis of this astrocentric orbit, a, is the sum of the semi-major axes of the star's orbit and the planet's orbit in the barycentric coordinates shown here.

In general, orbits under the inverse square force law are conic sections, the loci obtained by intersecting a cone with a plane. For planets, the orbits must be closed, i.e. they are either circular or, more generally, elliptical, with the eccentricity of the ellipse increasing as the misalignment of the normal to the plane with the axis of the cone increases. Of course, a circle is simply an ellipse with an eccentricity, e, of 0.

There is no physical significance to the cone or the plane; it simply happens that there is a mathematical coincidence.

The orbital period, P, the semi-major axis, a, and the star and planet masses are related by (the generalization of) **Kepler's third law**:

$$\frac{a^3}{P^2} = \frac{G(M_* + M_P)}{4\pi^2}, \tag{1.1}$$

where $a = a_* + a_P$ as indicated in Figure 1.12.

The Sun constitutes over 99.8% of the Solar System's mass, so the barycentre of the Solar System is close to, but not exactly at, the Sun's own centre of mass. As the planets orbit around the barycentre, the Sun executes a smaller **reflex orbit**, keeping the centre of mass of the system fixed at the barycentre.

In general, the motion of a star in a reflex orbit has a semi-major axis, a_*, that can, in principle, be detected as an angular displacement, β, when the star is viewed from distance d. This angle of the astrometric wobble, β, is proportional to the semi-major axis of the star's reflex orbit:

$$\beta = \frac{a_*}{d}.$$

However, since

$$a_* = \frac{M_P}{M_*} a_P,$$

we have

$$\beta = \frac{M_P a_P}{M_* d}, \tag{1.2}$$

and we see from Equation 1.2 that the astrometric wobble method is most effective for finding high-mass planets in wide orbits around nearby relatively low-mass stars.

Worked Example 1.1

(a) Calculate the orbital semi-major axis, $a_\odot$, of the Sun's reflex orbit in response to Jupiter's orbital motion. The mass of Jupiter, M_J, is 1.90×10^{27} kg, the mass of the Sun is 1.99×10^{30} kg, and Jupiter's orbital semi-major axis, a_J, is 7.784×10^{11} m. Jupiter constitutes about 70% of the mass in the Solar System apart from the Sun, so you may ignore the other lesser bodies in the system.

(b) Hence calculate the distance, d_{Gaia}, at which the astrometric wobble angle, β, due to the Sun's reflex orbit is greater than $\beta_{\text{Gaia}} = 10\,\mu$arcsec.

(c) State whether a Gaia satellite positioned anywhere within the sphere of radius d_{Gaia} would be able to detect the astrometric wobble due to the Sun's reflex orbit, explaining your reasoning.

(d) Comment on the fraction of the Galaxy's volume over which a hypothetical extraterrestrial Gaia could detect Jupiter's presence by the astrometry method.

Solution

(a) The barycentre of the Sun–Jupiter system is such that

$$M_J a_J = a_\odot M_\odot, \tag{1.3}$$

so

$$\begin{aligned} a_\odot &= \frac{M_J}{M_\odot} a_J = \frac{1.90 \times 10^{27}}{1.99 \times 10^{30}} \times 7.784 \times 10^{11}\ \text{m} \\ &= 7.432 \times 10^{8}\ \text{m}. \end{aligned}$$

The semi-major axis of the Sun's reflex orbit is 7.43×10^8 m.

(b) The distance d_{Gaia} is given by the small angle formula. To use this formula we must first convert the angle β_{Gaia} to radians:

$$\begin{aligned} 1 \times 10^{-5}\ \text{arcsec} &= 1 \times 10^{-5} \times \frac{2 \times \pi}{360 \times 60 \times 60}\ \text{rad} \\ &= 4.85 \times 10^{-11}\ \text{rad}. \end{aligned}$$

Here we have multiplied by the 2π radians in a full circle and divided by the $360 \times 60 \times 60$ arcseconds in a full circle, thus converting our angular units. Here π is *not* the parallax.

So $\beta_{\text{Gaia}} = 10\,\mu\text{arcsec} = 4.85 \times 10^{-11}$ rad. The astrometric wobble angle of the Sun's reflex orbit is given by

$$\beta = \frac{a_\odot}{d}, \tag{1.4}$$

so d_{Gaia} is given by

$$d_{\text{Gaia}} = \frac{a_\odot}{\beta_{\text{Gaia}}}. \tag{1.5}$$

Substituting values,

$$d_{\text{Gaia}} = \frac{a_\odot}{4.85 \times 10^{-11}} = \frac{7.43 \times 10^{8}}{4.85 \times 10^{-11}}\ \text{m} = 1.532 \times 10^{19}\ \text{m}.$$

Clearly the SI unit of metres is not a good choice for expressing interstellar distances, so we will express this distance in parsecs:

$$d_{\text{Gaia}} = \frac{1.532 \times 10^{19}\,\text{m}}{3.086 \times 10^{16}\,\text{m}\,\text{pc}^{-1}} = 4.96 \times 10^{2}\,\text{pc} = 496\,\text{pc}.$$

Hence the limiting distance is around $500\,\text{pc}$, to the one significant figure of the stated angular precision ($10\,\mu$arcsec).

(c) If the extraterrestrials' Gaia satellite is ideally positioned so that Jupiter's orbit is viewed face on, then the satellite will see the true elliptical shape of the Sun's reflex orbit. At any other orientation, the satellite will see a foreshortened shape; but even in the least favourable orientation, with **orbital inclination** $i = 90°$, as in Figure 1.13a, the satellite will see the Sun move back and forth along a line whose length is given by the size of the orbit. Only in the extremely unlucky case of a highly eccentric orbit, viewed from the least favourable inclination *and* azimuth, will the angular deviation be substantially less than that corresponding to the semi-major axis. Since Jupiter has a low orbital eccentricity, the extraterrestrial Gaia could detect the Sun's reflex wobble from anywhere within the sphere of radius d_{Gaia}.

The azimuth is the angle around the orbit: for a highly eccentric orbit, the projection on the sky will vary with azimuth, being smallest when the orbit is viewed from an extension of the semi-major axis.

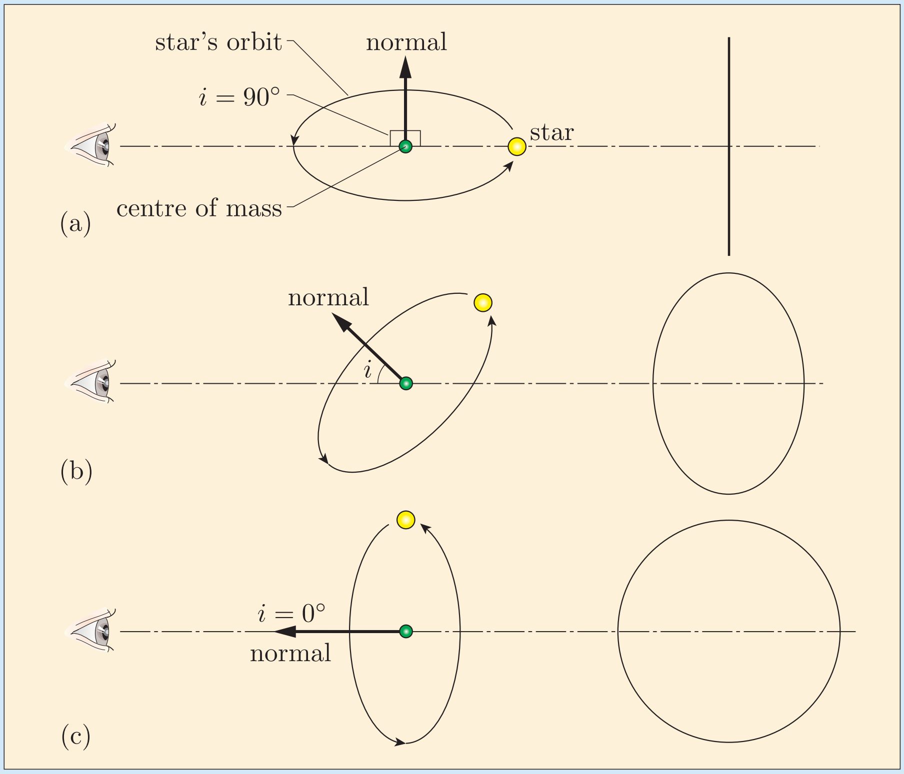

Figure 1.13 The shape of the orbit that the Gaia satellite sees is a function of the orbital inclination, i. In panel (a), $i = 90°$ and the orbit appears as a line traced on the sky. Panel (b) shows an intermediate value of i, and the orbit appears elliptical, with the true orbital shape being foreshortened. Panel (c) shows the situation where $i = 0°$; only in this case does the observer see the true shape of the orbit.

(d) The distance d_{Gaia} is about 500 pc, i.e. about 1500 ly. Comparing this with Figure 1.3a, we can see that this length scale is comparable to the width of the spiral arm structure in the Galaxy. The astrometric wobble of the Sun due to Jupiter's pull could be detected by advanced, spacecraft-building extraterrestrial civilizations in the same region of the Orion Arm as the Sun. The astrometric wobble would be too small to be detected by a Gaia-like satellite built by more remote extraterrestrials.

- How does the semi-major axis of the Sun's reflex orbit in response to Jupiter, $a_\odot$, compare with the solar radius, $R_\odot$? What does this imply for the position of the barycentre of the Solar System?
- The value of $R_\odot$ is 6.96×10^8 m, which is only just smaller than the value that we calculated for $a_\odot$, namely 7.43×10^8 m. This means that the barycentre of the Solar System is just outside the surface of the Sun.
- Will the barycentre of the Solar System remain at the same distance from the centre of the Sun as the eight planets in the Solar System all orbit around the barycentre? Explain your answer.
- No, the eight planets all have different orbital periods, so sometimes they will all be located on the same side of the Sun. When this happens, the barycentre will be pulled further from the centre of the Sun than the value that we calculated using Jupiter alone. At some other times most of the seven lesser planets will be on the opposite side of the Sun from Jupiter, in which case they will pull the barycentre closer to the centre of the Sun than implied by our calculations using Jupiter alone.
- For astrometric discovery prospects, is there any disadvantage inherent in a planet having a wide orbit?
- While the size of the astrometric wobble increases as the planet's semi-major axis increases, so too does the orbital period (i.e. the planet's 'year'). Kepler's third law tells us that $P \propto a^{3/2}$, so as the orbital size increases, the length of time required to measure a whole orbit increases even faster.

Our calculations show that our hypothetical extraterrestrial astronomers would be able to detect Jupiter's presence so long as they were within about 500 pc of the Sun and were able to construct an instrument with Gaia's capabilities. We do not yet know how common planetary systems like our own are, but once Gaia is launched we will begin to find out!

1.3 Radial velocity measurements

Like the astrometric method, the radial velocity method of planet detection relies on detecting the host star's reflex orbit. In this case, rather than detecting the change in position of the host star as it progresses around its orbit, we detect the change in velocity of the host star. The radial velocity, i.e. the velocity of an object directly towards or away from the observer, can be sensitively measured using the Doppler shift of the emitted light. This has been a powerful technique in many areas of astrophysics and was adopted in the 1980s by astronomers searching for Jupiter-like planets around nearby Sun-like stars.

1.3.1 The stellar reflex orbit with a single planet

The motion of a planet is most simply analyzed in the rest frame of the host star, i.e. the **astrocentric frame**. In this frame the planet executes an orbit with semi-major axis a, period P and eccentricity e, as shown in Figures 1.12b and 1.14.

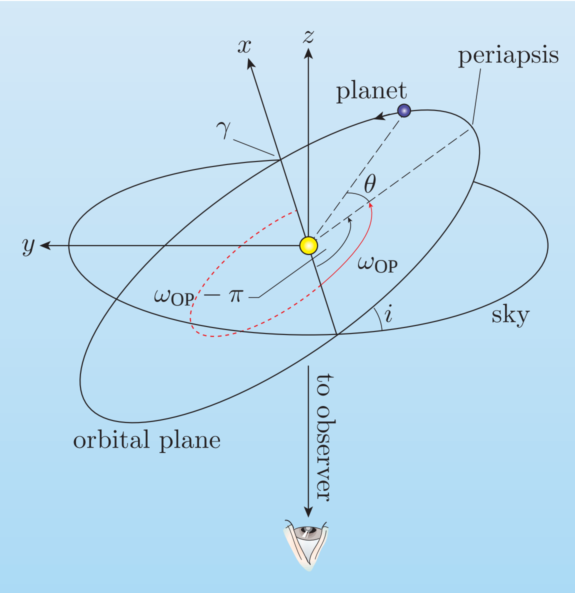

Figure 1.14 The astrocentric orbit of a planet. The observer is positioned in the direction of the bottom of the page, and is viewing the system along the direction of the z-axis. The x-axis is in the plane of the sky and is oriented so that it intersects the planet's orbit at the point where the z-component of the planet's velocity is towards the observer. Finally, the y-axis is the third direction making up a right-handed Cartesian coordinate system. The planet is closest to the star at the pericentre, whose position is defined by the angle $\omega_{\rm OP}$.

The point at which the planet is closest to the star is called the **pericentre**, and the star is positioned at one focus of the elliptical orbit. We will adopt a Cartesian coordinate system, centred on the host star, oriented as shown in Figure 1.14. The angle between the plane of the sky and the plane of the orbit is the orbital inclination, i. The x-axis is defined by the intersection of the orbit with the plane of the sky as seen by the observer. Positive x is on the side of the orbit where the planet moves towards the observer. The point labelled γ is the intersection of the orbit with the positive x-axis. The angle θ is the **true anomaly**, which measures how far around the orbit from the pericentre the planet has travelled. This angle is measured at the position of the host star. The angle $\omega_{\rm OP}$ measures the orientation of the pericentre with respect to γ. The velocity, $\boldsymbol{v}$, has components in the x-, y- and z-directions that are given by

$$\begin{aligned}
v_x &= -\frac{2\pi a}{P\sqrt{1-e^2}}\left(\sin(\theta+\omega_{\rm OP}) + e\sin\omega_{\rm OP}\right),\\
v_y &= -\frac{2\pi a\cos i}{P\sqrt{1-e^2}}\left(\cos(\theta+\omega_{\rm OP}) + e\cos\omega_{\rm OP}\right),\\
v_z &= -\frac{2\pi a\sin i}{P\sqrt{1-e^2}}\left(\cos(\theta+\omega_{\rm OP}) + e\cos\omega_{\rm OP}\right).
\end{aligned} \tag{1.6}$$

What astronomers can actually observe is the star, not the planet, so we need the analogous equations for the reflex orbit of the star. So far we've considered the orbit of the planet around the star, i.e. in an 'astrocentric' frame. The star is actually moving too, executing its reflex orbit around the barycentre, as illustrated in Figure 1.12a.

The velocity, $\boldsymbol{v}$, of the planet in the astrocentric frame (Figure 1.12b) is given by simple vector subtraction:

$$\boldsymbol{v} = \boldsymbol{v}_{\mathrm{P,bary}} - \boldsymbol{v}_*, \tag{1.7}$$

where $\boldsymbol{v}$ is the astrocentric velocity given in Equation 1.6, and $\boldsymbol{v}_*$ is the velocity of the star in the barycentric frame, i.e. the velocity of the star as it performs its reflex orbit about the barycentre as shown in Figure 1.12a. Equation 1.3 gave us the ratio of the semi-major axes of the orbit of a planet and the reflex orbit of its star. The relationship is much more general than our use of it in Section 1.2: for any planetary system, the barycentre remains fixed in its own inertial frame, so at all times the distances of the star and the planet from the barycentre will vary proportionately:

$$M_* \boldsymbol{r}_* = -M_{\mathrm{P}} \boldsymbol{r}_{\mathrm{P}}. \tag{1.8}$$

Here we have used vector notation, and since the planet and the star are in opposite directions from the barycentre, this equation introduces a minus sign into Equation 1.3, which used the (scalar) distance rather than the vector displacement. Differentiating with respect to time, we then obtain the general relationship, in the barycentric frame, between the velocities of the planet and the star's reflex orbit:

$$M_* \boldsymbol{v}_* = -M_{\mathrm{P}}\, \boldsymbol{v}_{\mathrm{P,bary}}. \tag{1.9}$$

- What do Equations 1.8 and 1.9 imply for the shapes of the two ellipses in Figure 1.12a?

- The ellipses are the same shape, and differ only in size.

Consequently, using Equation 1.9 to substitute for $\boldsymbol{v}_{\mathrm{P,bary}}$ in Equation 1.7, and making the barycentric velocity of the star the subject of the resulting equation, we obtain

The fraction multiplying $\boldsymbol{v}$ is known as the **reduced mass** of the planet, and is analogous to that quantity in simple two-body problems in other areas of physics.

$$\boldsymbol{v}_* = -\frac{M_{\mathrm{P}}}{M_{\mathrm{P}} + M_*}\boldsymbol{v}, \tag{1.10}$$

where $\boldsymbol{v}$ is the astrocentric orbital velocity of the planet, as given in Equations 1.6. Finally, we should note that in general the barycentre of the planetary system being observed will have a non-zero velocity, $\boldsymbol{V}_0$, with respect to the observer. $\boldsymbol{V}_0$ changes on the timescale of the star's orbit around the centre of the Galaxy, i.e. hundreds of Myr. Thus we can regard it as a constant as this timescale is much longer than the timescale for the orbits of planets around stars. From the point of view of an observer in an inertial frame, therefore, the reflex velocity of the star is $\boldsymbol{V} = \boldsymbol{v}_* + \boldsymbol{V}_0$. So we now have a completely general expression, in the frame of an inertial observer, for the reflex velocity of a star in response to the motion of a planet around it:

$$\begin{aligned}
V_x &= V_{0,x} + \frac{2\pi a M_{\mathrm{P}}}{(M_{\mathrm{P}} + M_*)P\sqrt{1-e^2}}\left(\sin(\theta + \omega_{\mathrm{OP}}) + e\sin\omega_{\mathrm{OP}}\right), \\
V_y &= V_{0,y} + \frac{2\pi a M_{\mathrm{P}}\cos i}{(M_{\mathrm{P}} + M_*)P\sqrt{1-e^2}}\left(\cos(\theta + \omega_{\mathrm{OP}}) + e\cos\omega_{\mathrm{OP}}\right), \\
V_z &= V_{0,z} + \frac{2\pi a M_{\mathrm{P}}\sin i}{(M_{\mathrm{P}} + M_*)P\sqrt{1-e^2}}\left(\cos(\theta + \omega_{\mathrm{OP}}) + e\cos\omega_{\mathrm{OP}}\right).
\end{aligned} \tag{1.11}$$

- How do the three components of $\boldsymbol{V}$ contribute to the observed stellar radial velocity?
- The radial velocity is the motion directly towards or away from the observer. The coordinate system that we adopted has the z-axis directed away from the observer, while the x- and y-axes are in the plane of the sky. The radial velocity is given by V_z. The other two components do not contribute to the radial velocity.
- Which of the terms in the expression for the stellar radial velocity are time-dependent? Describe in simple physical terms how the time-dependence arises.
- The only time-dependent term in the expression for V_z is the true anomaly, i.e. the angle $\theta(t)$, which changes continuously as the planet and star proceed along their orbits around the barycentre.

Exercise 1.3 Use Kepler's third law to estimate the time for the Sun to orbit around the Galaxy. You may assume the mass of the Galaxy is $10^{12}\,\mathrm{M}_\odot$ and may be approximated as a point mass at the centre of the Galaxy, and that the distance of the Sun from the centre of the Galaxy (known as the **Galactocentric distance**) is 8 kpc. ■

The radial velocity, which we will henceforth simply call V, of a star executing a reflex motion as a result of a single planet in an elliptical orbit is given by

$$V(t) = V_{0,z} + \frac{2\pi a M_\mathrm{P} \sin i}{(M_\mathrm{P} + M_*)P\sqrt{1-e^2}}\left(\cos(\theta(t) + \omega_\mathrm{OP}) + e\cos\omega_\mathrm{OP}\right). \quad (1.12)$$

$\theta(t)$ completes a full cycle of 360° (or 2π radians) each orbit. Unless the orbit is circular, θ does not change linearly with time; instead, it obeys Kepler's second law, or equivalently the **law of conservation of angular momentum**.

Exercise 1.4 Use Equation 1.12 for the radial velocity to answer the following.

(a) What is the dependence of the observed radial velocity variation on the orbital inclination, i? State this dependence as a proportionality, and draw diagrams illustrating the values of i for the maximum, the minimum and an intermediate value of the observed radial velocity. You may assume that all the characteristics of the observed planetary system, except for its orientation, remain constant.

(b) For fixed values of all parameters except the orbital eccentricity, e, how does the amplitude of the observed radial velocity variation change as the eccentricity varies? (By definition, the eccentricity of an ellipse lies in the range $0 \leq e \leq 1$.) Explain your answer fully, with reference to the behaviour of the relevant terms in Equation 1.12.

(c) Adopting the approximation that Jupiter is the only planet in the Solar System, calculate the observed radial velocity amplitude, A_RV, for the Sun's reflex orbit. Express your answer as a function of the unknown orbital inclination, i. Use the following (approximate) values of constants to evaluate your answer: $\mathrm{M_J} = 2\times10^{27}$ kg, $\mathrm{M}_\odot = 2\times10^{30}$ kg, $\mathrm{a_J} = 8\times10^{11}$ m; Jupiter's orbital period is $\mathrm{P_J} = 12$ years, and its orbital eccentricity is $\mathrm{e_J} = 0.05$. ■

An important result from Exercise 1.4 is that the amplitude of the reflex radial velocity variations predicted by Equation 1.12 is

$$A_{\mathrm{RV}} = \frac{2\pi a M_{\mathrm{P}} \sin i}{(M_{\mathrm{P}} + M_{*}) P \sqrt{1 - e^2}}. \tag{1.13}$$

Applying this to the Sun's reflex orbit due to Jupiter, we find a radial velocity amplitude of $A_{\mathrm{RV}} \leq 13\,\mathrm{m\,s^{-1}}$.

Astronomers measure radial velocities using the Doppler shift of the features in the stellar spectrum. The wavelength change, $\Delta\lambda$, due to the Doppler shift is given by

$$\frac{\Delta\lambda}{\lambda} = \frac{V}{c}, \tag{1.14}$$

so to detect the reflex orbit of the Sun due to Jupiter's presence, our hypothetical extraterrestrial astronomers would need to measure the wavelength shifts of features in the solar spectrum to a precision of

$$\frac{\Delta\lambda}{\lambda} = \frac{13\,\mathrm{m\,s^{-1}}}{3.0 \times 10^8\,\mathrm{m\,s^{-1}}} = 4.2 \times 10^{-8},$$

where we have substituted the value for the speed of light, c, in SI units. This sounds challenging, but it is possible with current technology; terrestrial astronomers have aspired to this since the 1980s. For bright stars with prominent spectral features it is now possible to measure radial velocities to precisions of better than $1\,\mathrm{m\,s^{-1}}$, i.e. motions slower than walking speed can be detected! Figure 1.15 shows the radial velocity measurements used to infer the presence of the planet around GJ 832 (also known as HD 204691); this planet has a lower mass than Jupiter and has $P = 9.4$ years. GJ 832's reflex radial velocity amplitude slightly exceeds that of Jupiter because, as we saw in Table 1.1, the star has mass less than half that of the Sun, and the planet has a shorter orbital period than Jupiter. Our Sun happens to have a spectral type (G2V) that makes it particularly suitable for radial velocity measurements: it has a host of sharp, well-defined photospheric absorption lines. By measuring the shifts in the observed wavelengths of these lines, our hypothetical extraterrestrial astronomers would be able to detect the presence of Jupiter unless they happen to be unlucky and view the Sun–Jupiter system from an orbital inclination, i, close to $0°$. The other limiting factor, assuming that they have technology comparable to ours, is their distance from the Sun. To make radial velocity measurements of the required precision, astronomers need to collect a lot of light, and as noted previously the flux of photons from the Sun drops off as $1/d^2$.

GJ 832 is one of the 100 nearest known stars listed Table 1.1.

Exoplanet naming convention

The planet discovered around the star GJ 832 is called GJ 832 b. This is the general convention: the first exoplanet discovered around any star is given its host star's name with 'b' appended. The second planet discovered in the system is labelled 'c', and so on. This distinguishes planets from stellar companions, which have capital letters appended: for example, the stars α Cen A and α Cen B. The planets in a multiple planet system are always labelled b, c, d, ... *in the order of discovery*; the distances of these planets from the host star can consequently be in any order.

- If a planet were discovered orbiting around the star α Cen A, what would it be called?
- Assuming that it was the first planet discovered orbiting around the star, it would have the star's name with 'b' appended: α Cen A b.

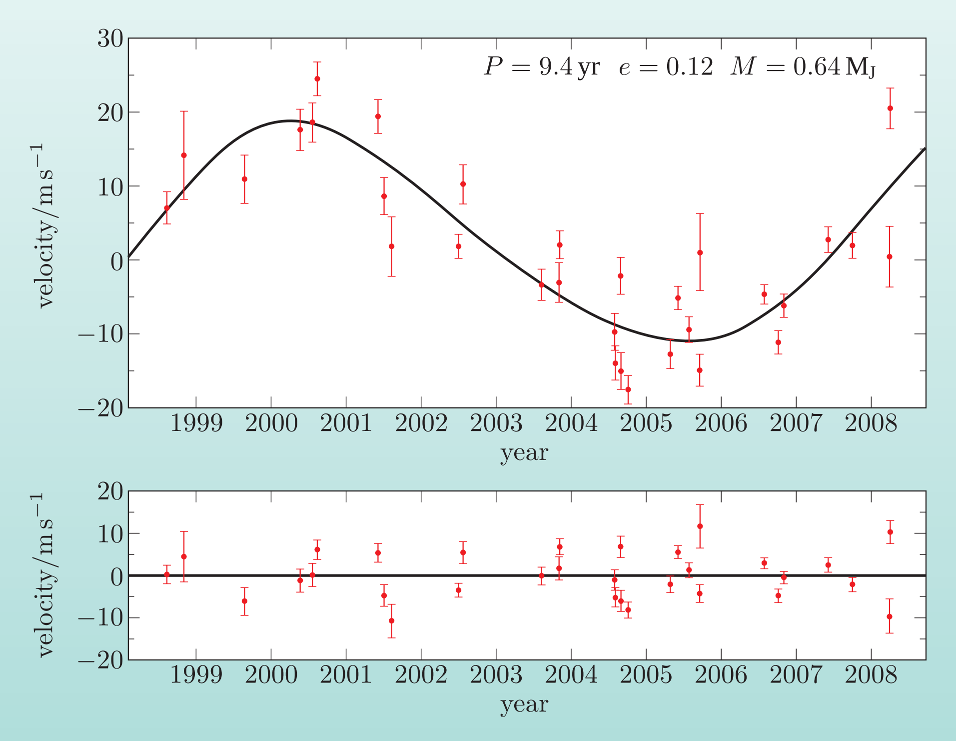

Figure 1.15 Upper panel: radial velocity measurements revealing the presence of the planet around GJ 832, with the best-fitting solution of the form of Equation 1.12 overplotted as a dashed line. The parameters corresponding to this fit for the planet GJ 832 b are indicated. This planet's orbit has similarities to that of Jupiter. Lower panel: the deviations of the measured data points from the best-fitting solution.

Figure 1.15 shows radial velocity measurements as a function of time. The best-fitting model solution, which is overplotted, was generated using Equation 1.12. If we examine Equation 1.12, we see that it predicts the same value for $V(t)$ every time $\theta(t)$ completes a full cycle, i.e. every time the star returns to the same position on its orbit. In the case of GJ 832 b, the orbital period is long, and it is easy to make observations sampling each part of the orbit. For shorter orbital periods, sometimes only a single measurement is made during a particular orbit; to make a graph like Figure 1.15, many orbits would need to be plotted on the horizontal axis, and the plotted points would be very thinly spread out. A more efficient way of presenting such data is to **phase-fold**, so that instead of plotting time on the horizontal axis, one plots **orbital phase**, ϕ:

$$\phi = \frac{t - T_0}{P} - N_{\rm orb}, \tag{1.15}$$

The timetable giving orbital phase for any value of time, t, is known as an **ephemeris**.

where t is time; T_0 is a **fiducial** time, for example, T_0 could be fixed at the first observed time at which the star is farthest from the observer; P is the orbital period; and N_{orb} is an integer such that $0 \leq \phi \leq 1$. As the star proceeds around a full orbit, t increases by an amount equal to the orbital period, P, and ϕ covers the full range of values $0 \leq \phi \leq 1$. Once per orbit, when the star crosses the fiducial point corresponding to T_0, the integer N_{orb} increments its count: N_{orb} is known as the **orbit number**.

At first glance the curve shown in Figure 1.15 looks very much like the familiar sinusoidal curve that one expects to see whenever there is motion in a circle. If you look carefully, however, you should see that the curve does not have the perfect symmetries of a sine curve: it corresponds to an orbit with finite eccentricity, $e = 0.12$. For more extreme values of the eccentricity, the deviations from a sine curve become more pronounced, as shown in Figure 1.16. The eccentricities of the solutions shown in Figure 1.16 range from $e = 0.17$ for HD 6434 to $e = 0.41$ for HD 65216.

Exercise 1.5 In Exercise 1.4 we found that the amplitude of the stellar reflex orbit's radial velocity is

$$A_{\mathrm{RV}} = \frac{2\pi a M_{\mathrm{P}} \sin i}{(M_{\mathrm{P}} + M_*)P\sqrt{1-e^2}}. \qquad \text{(Eqn 1.13)}$$

(a) This equation has the orbital semi-major axis in the numerator, so at first glance it appears that the radial velocity amplitude increases as the planet's orbital semi-major axis increases. Does A_{RV} in fact increase as a planet's orbital semi-major axis increases? Explain your reasoning.

(b) State, with reasoning, how the radial velocity amplitude depends on planet mass, star mass, semi-major axis and eccentricity. ■

1.3.2 Reflex radial velocity for many non-interacting planets

So far we have only considered a single planet. For more than one planet, so long as the planets do not significantly perturb each other's elliptical orbits, we can simply combine all of the elliptical reflex orbits about the barycentre. The observed radial velocity will be

$$V = V_{0,z} + \sum_{k=1}^{n} A_k \left(\cos(\theta_k + \omega_{\mathrm{OP},k}) + e_k \cos \omega_{\mathrm{OP},k}\right), \qquad (1.16)$$

where there are n planets, each with their own mass, M_k, and **instantaneous orbital parameters** a_k, e_k, θ_k and $\omega_{\mathrm{OP},k}$, and their own instantaneous value of A_k given by

$$A_k = \frac{2\pi a_k M_k \sin i}{M_{\mathrm{total}} P_k \sqrt{1-e_k^2}}, \qquad (1.17)$$

where M_{total} is the sum of the masses of the n planets and the star. Generally, Equation 1.16 is an approximation. The instantaneous orbital parameters will evolve over several cycles of the longest planet's period because of the gravitational interactions between the planets.

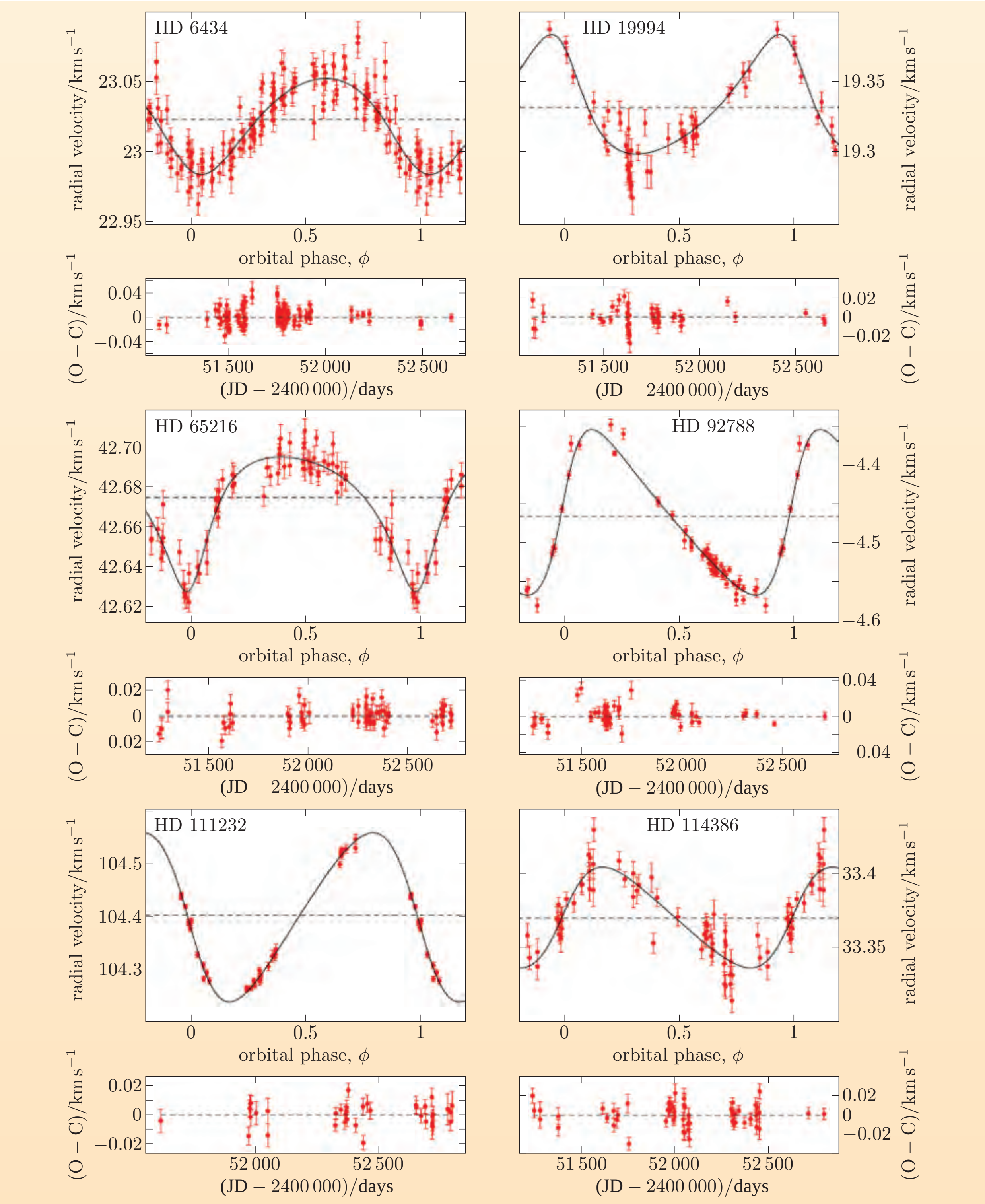

Figure 1.16 Radial velocity measurements and best-fitting solutions of the form of Equation 1.12. Upper panels: radial velocity measurements and solutions folded and plotted as a function of orbital phase. Lower panels: the deviations of the measured data points from the best-fitting solution, plotted as a function of time. Data are shown for six different stars, illustrating some of the many diverse curves that are described by Equation 1.12. '(O − C)' denotes 'observed' minus 'calculated' and indicates how well the model fits the measurements.

- What conditions are required for Equation 1.16 to be valid?

- The planets' mutual gravitational attraction at all times must be negligible compared to the gravitational force exerted by the central star on each planet. This requires the planets to all be of small mass compared to the star, and to have large orbital separations. If this is not the case, the simple two-body solution for the astrocentric orbit of the planet will not be valid.

Figure 1.17 shows two examples of two-planet fits using Equation 1.16. In the case of HD 82943, the planet inducing the larger-amplitude reflex motion has approximately twice the orbital period of the second planet, so a pattern of alternating extreme and less extreme negative radial velocity variations is produced. In the case of HD 169830, the shorter-period planet completes about seven orbits for one orbit of the longer-period planet. This figure demonstrates how continued monitoring of the radial velocities of known planet hosts can reveal the existence of additional planets.

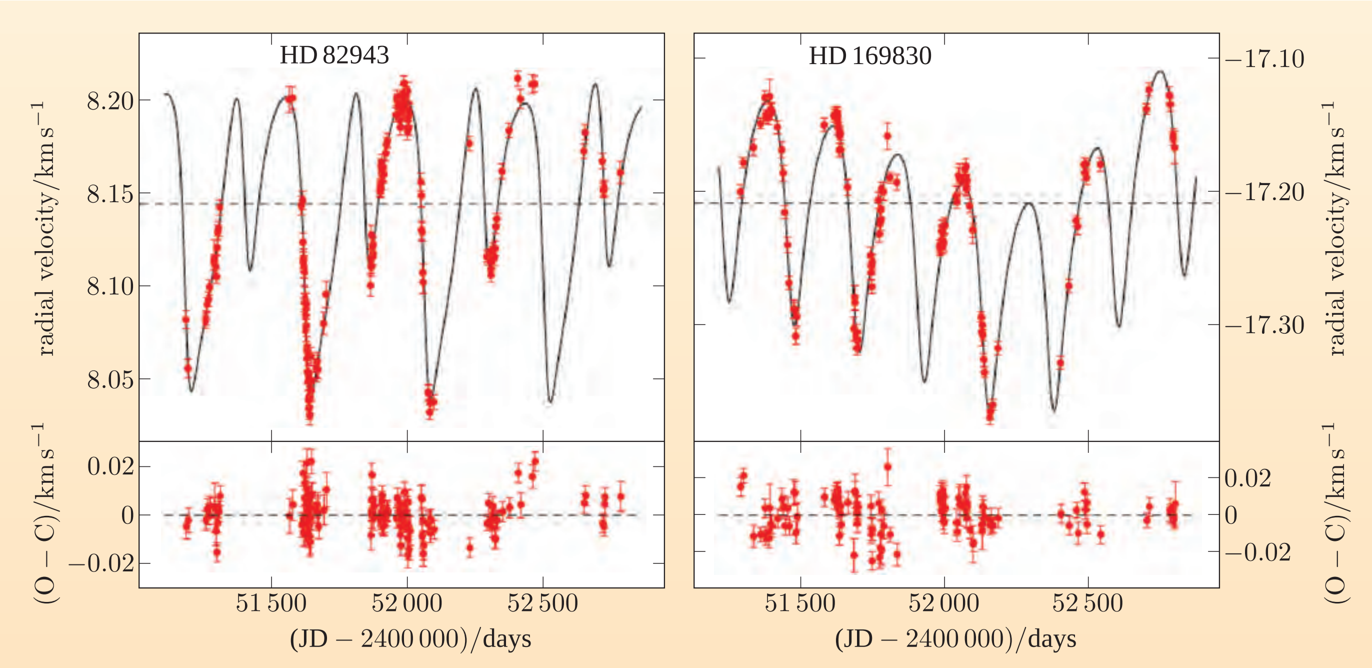

Figure 1.17 Radial velocity measurements and best-fitting solutions of the form of Equation 1.16 for two planets overplotted. Upper panels: radial velocity measurements and solutions plotted as a function of time. Lower panels: the deviations of the measured data points from the best-fitting solution, plotted as a function of time. Data are shown for two different stars, illustrating two of the many diverse curves that are described by Equation 1.16.

The radial velocity technique has been extremely successful in detecting planets around nearby stars. The majority of known exoplanets (October 2009) were detected using it. The technique is limited in its applicability in two significant ways: it can measure the radial velocity precisely only if the stellar spectrum contains suitable features, and only if the star appears bright enough. Even for the brightest of planet host stars, current telescopes can only make precise enough velocity measurements for stars within ∼2000 pc (or ∼6000 light-years). Finally, the results from radial velocity measurements all carry the unknown factor $\sin i$, unless the orbital inclination, i, can be determined using some other method.

1.4 Transits

The transit technique is second only to direct imaging in its simplicity. Figure 1.18 shows transits of Venus and Mercury: when a planet passes in front of the disc of a star, it blocks some of the light that the observer would normally receive.

(a) (b)

Figure 1.18 Photographs of transits of (a) Venus and (b) Mercury as observed from Earth on partially cloudy days.

Thus the presence of an opaque object orbiting around a star may be inferred if the star is seen to dip in brightness periodically. The size of the dip in brightness expected during the transit can be estimated simply from the fraction of the stellar disc covered by the planet:

$$\frac{\Delta F}{F} = \frac{R_{\mathrm{P}}^2}{R_*^2}. \tag{1.18}$$

Here F is the flux measured from the star, and ΔF is the observed change in this flux during the transit. The right-hand side is simply the ratio of the areas of the planet's and star's discs. Equation 1.18 gives us a straightforward and joyous result: if a planet transits its host star, we immediately have an estimate of the size of the planet, in terms of the size of its host star. Equation 1.18 applies when the host star is viewed from an interstellar distance. The geometry for transits of Solar System planets viewed from Earth is slightly more complicated.

- Generally, the fraction of a background object obscured by a smaller foreground object depends on the relative distances of the two objects from the observer; for example, it is easy to obscure the Moon with your fist. Why does Equation 1.18 not need to account for the relative distances of the star and planet from the observer?

- As we noted in the Introduction, the distances between stars are very much larger than the typical sizes of planetary orbits. Thus the distance between any observer and an exoplanet is identical to high precision to the distance between the same observer and the host star. Expressed geometrically, the rays of light reaching the observer from the exoplanet host star are parallel, so Equation 1.18 holds.

1.4.1 Transit depth for terrestrial and giant planets

Equation 1.18 allows us to calculate the depth of the transit light curve that would be observed by our hypothetical extraterrestrial astronomers for any of the Solar System planets. For example, the Earth transiting the Sun would cause a dip

$$\frac{\Delta F_\mathrm{E}}{F} = \frac{\mathrm{R}_\oplus^2}{\mathrm{R}_\odot^2} = \left(\frac{6.4\times 10^3\ \mathrm{km}}{7.0\times 10^5\ \mathrm{km}}\right)^2$$
$$= 8\times 10^{-5},$$

where we have substituted in the values of the radius of the Earth, $\mathrm{R}_\oplus$, and the radius of the Sun, $\mathrm{R}_\odot$, to two significant figures, and reported the result to one significant figure. Similarly, a transit by Jupiter would cause a dip of

$$\frac{\Delta F_\mathrm{J}}{F} = \frac{\mathrm{R}_\mathrm{J}^2}{\mathrm{R}_\odot^2} = \left(\frac{7.0\times 10^4\ \mathrm{km}}{7.0\times 10^5\ \mathrm{km}}\right)^2$$
$$= 1\times 10^{-2}.$$

As a ‘rule of thumb’, a giant planet transit will cause a dip of $\sim$1% in the light curve of the host star, while a terrestrial planet transit will cause a dip of $\sim 10^{-2}$%. The first of these figures is easily within the precision of ground-based photometric instruments. In fact, in the 1950s Otto Struve predicted that transits of Jupiter-like exoplanets could be detected if such planets were orbiting at favourable orbital inclinations. The transit depth for a terrestrial planet is 100 times smaller, and requires a photometric precision of better than 10^{-4}. This is impossible to obtain reliably from Earth-bound telescopes because of the constantly changing transparency of the Earth’s atmosphere. For this reason, while there are scores of known transiting giant exoplanets, we know of only one transiting terrestrial planet, CoRoT-7 b, though we believe that the discovery of another is about to be announced (December 2009). Further discoveries are anticipated imminently as the French/ESA satellite CoRoT continues its mission, the NASA Kepler satellite begins announcing results, and the first transit surveys optimized for M dwarf stars produce results. Further space missions are being designed specifically to find terrestrial planets; we will discuss them in Chapter 8.

- ● If an astronomer detects a regular 1% dip in the light from a star, can they immediately conclude that they have detected a transiting Jupiter-sized planet orbiting around that star?
- ❍ No. The conclusion can only be that there is a Jupiter-sized opaque body orbiting the star. To prove that this body is a planet, rather than, for example, a brown dwarf star, the mass of the transiting body needs to be ascertained.
- ● How can the astronomer ascertain the mass of the object that is transiting the star?
- ❍ By using the radial velocity technique described in Section 1.3.
- ● Why are M dwarf stars particularly promising for the discovery of terrestrial planet transits?
- ❍ M dwarfs are the smallest stars, so a small planet produces a relatively large transit signal in an M dwarf, as Equation 1.18 shows.

The transit technique is extremely powerful; however, radial velocity confirmation of planet status is vital for transit candidates. The transiting extrasolar planets are the *only* planets outside our own Solar System with directly measured sizes. Fortunately, the transit technique and the radial velocity technique are beautifully complementary: radial velocity measurements allow the mass of the transiting body to be deduced, while the presence of transits immediately constrains the value of the orbital inclination, i, thus removing the major uncertainty in the interpretation of radial velocity measurements. For the transiting extrasolar planets, therefore, it is possible to deduce accurate and precise masses, radii and a whole host of other quantities. This wealth of empirical information makes the transiting planets invaluable, and underpins our choice of subjects for this book.

1.4.2 Geometric probability of a transit

How likely are our hypothetical extraterrestrial astronomers to discover transits of the Solar System planets? A transit will be seen if the orbital plane is sufficiently close to the observer's line of sight. Figure 1.19 illustrates the geometry of this situation; for the purpose of this discussion we will assume a circular orbit.

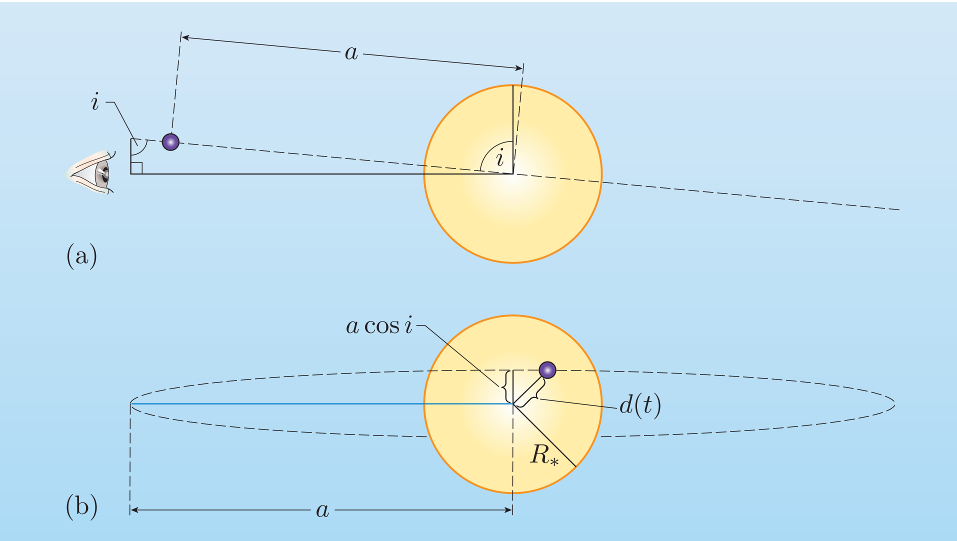

Figure 1.19 (a) The geometry of a transit as viewed from the side. The distant observer (not seen) views the system with orbital inclination i. (b) The geometry of the system from the observer's viewing direction. Note that the observer does not 'see' this geometry: the star is an unresolved point source.

For a transit to be seen, the disc of the planet must pass across the disc of the star. Referring to Figure 1.19b, the closest approach of the centre of the planet's disc to the centre of the star's disc occurs at inferior conjunction, when the planet is closest to the observer. At this orbital phase, by convention referred to as phase $\phi = 0.0$, the distance between the centres of the two discs is

$$d(\phi = 0.0) = a \cos i. \tag{1.19}$$

Note that here and throughout this book, a is the semi-major axis of the orbit; in this case we are assuming a circular orbit, so a is simply the radius of the transiting planet's orbit.

Note: the right-hand side of Equation 1.19 is *not* the arccosine function (which is sometimes typeset as acos).

For the planet's disc to occult the star's disc, therefore, the orbital inclination, i, must satisfy

$$a\cos i \leq R_* + R_\mathrm{P}. \tag{1.20}$$

- What happens if $R_* - R_\mathrm{P} < a\cos i \leq R_* + R_\mathrm{P}$? Would the transit depth be given by Equation 1.18 in this case?

- For $R_* - R_\mathrm{P} \leq a\cos i \leq R_* + R_\mathrm{P}$, we have a grazing transit: the disc of the planet only partially falls in front of the disc of the star, so a transit is observed, but its depth is less than that give by Equation 1.18 because a smaller area of the stellar disc is occulted.

The projection of the unit vector normal to the orbital plane onto the plane of the sky is $\cos i$, and is equally likely to take on any random value between 0 and 1. To simplify notation below, we temporarily replace the variable $\cos i$ with x. For the purposes of our discussion we will assume that our extraterrestrial astronomers have the necessary technology and are located in a random direction. Thus the probability of our extraterrestrials detecting a transit of a particular Solar System planet is the probability that the random inclination satisfies Equation 1.20:

$$\begin{aligned}\text{geometric transit probability} &= \frac{\text{number of orbits transiting}}{\text{all orbits}}\\ &= \frac{\int_0^{(R_*+R_\mathrm{P})/a}\mathrm{d}x}{\int_0^1\mathrm{d}x},\end{aligned}$$

so

$$\text{geometric transit probability} = \frac{R_* + R_\mathrm{P}}{a} \approx \frac{R_*}{a}. \tag{1.21}$$

Equation 1.21 shows that transits are most probable for planets with small orbits and large parent stars.

The probability for transits being observable is small; as Figure 1.20 shows, it is less than 1% for all of the Solar System's planets except Mercury. It is rather unlikely that our hypothetical extraterrestrial astronomers would be fortunate enough to observe transits for any of the Solar System's planets.

1.5 Microlensing

Gravitational microlensing exploits the lensing effect of the general relativistic curvature of spacetime to detect planets. For the effect to occur, a chance alignment of stars from the point of view of the observer is required. These alignments do occur from time to time, and are most frequent if one looks at regions of the Galaxy that are densely populated with stars. Terrestrial astronomers working on microlensing observe in the directions of regions that are densely populated with stars. The most obvious and best-studied of these is the **Galactic bulge**: the dense region of stars around the centre of our Galaxy. The bulge of the nearest external spiral galaxy, M31, has also been targeted, as have the Magellanic Clouds. Over 2000 microlensing events have been observed in the Galactic bulge studies, and in a handful of these events, planets have been detected around the foreground, lensing star.

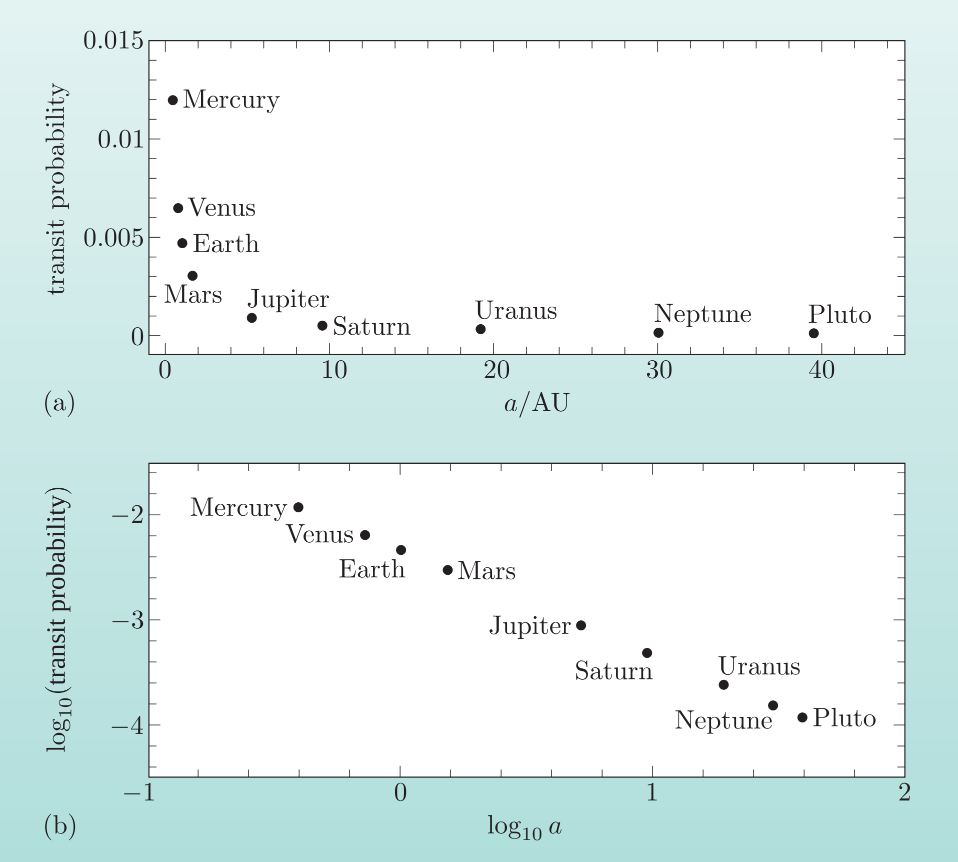

Figure 1.20 The probability of transits of each of the Solar System planets being observable for randomly positioned extraterrestrials. (a) The probability drops off as a^{-1}, and even for Mercury is only just over 1%. (b) Plotted on a $\log(\text{probability})$ versus $\log(a)$ graph, the relationship is a straight line of gradient -1.

Figure 1.21 shows our position relative to the Galactic bulge. The planets detected by microlensing are positioned just on our side of the Galactic bulge. Since the Sun is positioned towards the edge of the Milky Way Galaxy, as shown in Figure 1.21, to view it against the dense stellar background of the Galactic bulge, an observer would need to be situated in the sparsely populated regions at the edge of the Galaxy.

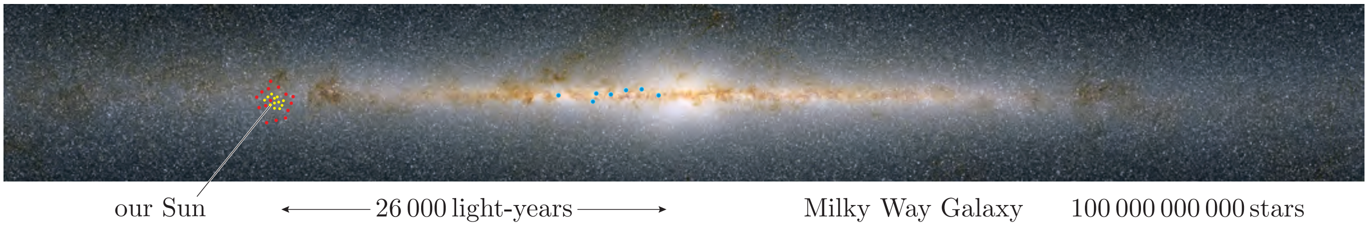

Figure 1.21 A side-on view of our Galaxy produced from a composite of 2MASS photometry, our Sun's distance from the centre is indicated. The dots schematically indicate the locations of exoplanets discovered by three primary methods of exoplanet discovery: yellow dots, radial velocity method; red dots, transits; blue dots, microlensing. The planets discovered by direct imaging are all very close to our Sun.

Since these regions have low abundances of elements heavier than He, and the density of stars there is low, this part of the Galaxy is *a priori* not the most likely to contain technological extraterrestrial civilizations. In addition, the probability of any given star becoming aligned with a background star and acting as a microlens is vanishingly small; this is a consequence of the very small size of stars compared to interstellar distances. Einstein realized this, and predicted in 1936 that microlensing would occur, though noting that 'there is no great chance of observing this phenomenon'. The reason why we have detected microlensing events is that modern technology permits continuous monitoring of millions of stars, to outweigh the vanishingly small probability ($\sim 10^{-6}$) of any individual star participating in a microlensing alignment at any particular time. Even Einstein could not have begun to anticipate the powerful technologies that have revolutionized astrophysics within the last half century. Putting the two factors together, i.e. the improbability of the Sun participating in a microlensing alignment and the expected dearth of technological extraterrestrials on the edges of the Milky Way, we can conclude that it is highly unlikely that Solar System planets would be detected by hypothetical extraterrestrial astronomers via the microlensing method.

Though it has detected only ten planets (December 2009), gravitational microlensing is important because it is the method that has found the majority of terrestrial exoplanets; recently, however, terrestrial mass planets have been discovered by both transit and radial velocity techniques (December 2009). Notably, gravitational microlensing may also have detected a planet in the galaxy M31; it is probably the only method that could conceivably detect planets outside the Milky Way. To offset these advantages, microlensing has the serious disadvantage that the lensing event is a one-off occurrence: there is no opportunity for confirming and refining the observations. This means that the parameters are rather ill-constrained, and can be meaningfully discussed only in a statistical sense. The statistical analysis of microlensing results implies that no more than a third of solar-type stars host giant planets. The topic of exoplanet detection by microlensing could easily fill an entire book; since we are focusing on transiting exoplanets, we exhort the interested reader to look elsewhere for these details.

Summary of Chapter 1

1. The Sun is one of the more luminous stars in the solar neighbourhood. The majority of objects within 10 parsecs are isolated M dwarf stars. Six of the nearest 100 stars (including the Sun) harbour known planets (October 2009).
2. The exoplanets in a multiple planet system are labelled b, c, d, ... *in the order of discovery*.
3. Direct imaging as a method for exoplanet detection is limited to bright planets in distant orbits around nearby faint stars. It is most effective in the infrared where the contrast ratio is favourable. A giant exoplanet has been discovered orbiting a brown dwarf using the direct imaging method.
4. A planet's light is composed of reflected starlight, which has a spectral energy distribution close to that of the host star, and a thermal emission component peaking at longer wavelengths.
5. The thermal emission from giant planets is partially powered by gravitational (Kelvin–Helmholtz) contraction. This emission is brightest for young giant planets.
6. A young planet has been detected around Fomalhaut using coronagraphy, and three young planets have been discovered around HD 8799. Exoplanet

imaging instruments like SPHERE and GPI should make further discoveries soon (October 2009).

7. The orbits of planets are elliptical. In astrocentric coordinates, the host star is at one focus of the ellipse. The orbital period, the semi-major axis, and the masses are related by Kepler's third law:

$$\frac{a^3}{P^2} = \frac{G(M_* + M_\mathrm{P})}{4\pi^2}. \qquad \text{(Eqn 1.1)}$$

The pericentre is the point on the planet's orbit that is closest to the star. The motion of the planet around the elliptical orbit is measured by the true anomaly, $\theta(t)$. The true anomaly is measured at the star, and is zero when the planet crosses the pericentre.

8. Both the host star and its planet(s) move about the barycentre (the centre of mass) of the system. For a single-planet system,

$$M_* \boldsymbol{r}_* = -M_\mathrm{P} \boldsymbol{r}_\mathrm{P}. \qquad \text{(Eqn 1.8)}$$

The reflex orbit of the star is, therefore, a scaled-down ellipse of the same eccentricity as the planet's orbit.

9. The reflex motion of the stellar orbit can be detected by astrometry. The Gaia satellite could detect the Sun's reflex orbital motion from a distance of about 500 pc, which is roughly the width of a spiral arm. Astrometry is most effective for massive planets in wide orbits around low-mass stars, but long-term monitoring is required to detect planets with large semi-major axes.

10. The orbital positions of the star and planet are uniquely defined by the orbital phase

$$\phi = \frac{t - T_0}{P} - N_\mathrm{orb}, \qquad \text{(Eqn 1.15)}$$

where t is time, T_0 is a fiducial time, and N_orb is the orbit number.

11. For a single planet, the amplitude of the stellar reflex radial velocity variation is

$$A_\mathrm{RV} = \frac{2\pi a M_\mathrm{P} \sin i}{(M_\mathrm{P} + M_*) P \sqrt{1 - e^2}}. \qquad \text{(Eqn 1.13)}$$

The largest radial velocity amplitudes are exhibited by low-mass host stars with massive close-in planets in eccentric orbits.

12. The radial velocity, V, of a star is given by

$$V = V_{0,z} + \sum_{k=1}^{n} A_k \left(\cos(\theta_k + \omega_{\mathrm{OP},k}) + e_k \cos \omega_{\mathrm{OP},k}\right), \qquad \text{(Eqn 1.16)}$$

where there are n planets, each with their own instantaneous parameters M_k, a_k, e_k, θ_k, $\omega_{\mathrm{OP},k}$, and A_k given by

$$A_k = \frac{2\pi a_k M_k \sin i}{M_\mathrm{total} P_k \sqrt{1 - e_k^2}}, \qquad \text{(Eqn 1.17)}$$

where M_total is the sum of the masses of the n planets and the star.

13. Radial velocity measurements using the Doppler shift of features in stellar spectra can be made to a precision less than $1\,\mathrm{m\,s^{-1}}$. The majority of known exoplanets (December 2009) were detected by the radial velocity method. This is the most likely method by which hypothetical extraterrestrials might detect the existence of the Sun's planets.

14. The depth of an exoplanet transit is

$$\frac{\Delta F}{F} = \frac{R_\mathrm{P}^2}{R_*^2}. \qquad \text{(Eqn 1.18)}$$

For Jupiter-sized and Earth-sized planets around a solar-type star, this depth is $\sim 1\%$ and $\sim 10^{-2}\%$, respectively.

15. The geometric transit probability is given by

$$\text{geometric transit probability} \approx \frac{R_*}{a}. \qquad \text{(Eqn 1.21)}$$

Transits are most likely for large planets in close-in orbits. If the Solar System were viewed from a random orientation, only Mercury, with $a = 0.4$ AU, has a transit probability exceeding 1%.

16. Terrestrial exoplanets have so far been detected primarily via the microlensing method, though they are now being discovered by the transit and radial velocity techniques (December 2009).

Acknowledgements

Grateful acknowledgement is made to the following sources:

Figures

Cover image: An artist's impression of the 'hot Jupiter' exoplanet HD 189733 b transiting across the face of its star (ESA, C. Carreau);

Figure 1: © Lynette R. Cook;

Figure 1.1: NASA Ames Research Center (NASA-ARC); Figures 1.2 and 1.3: Richard Powell, www.atlasoftheuniverse.com, used under a Creative Commons Attribution-ShareAlike 2.5 License; Figure 1.4; generated by the author from RECONs data; Figure 1.5a: adapted from a European Space Agency image; Figure 1.5b: The International Astronomical Union/Martin Kornmesser; Figure 1.5c: Lunar and Planetary Institute/NASA; Figures 1.6a & b and 1.7: NASA Jet Propulsion Laboratory (NASA-JPL); Figure 1.6c: NASA/Goddard Space Center; Figures 1.8 & 8.12: adapted from Kaltenegger, L. (2008) 'Assembling the Puzzle — Evolution of an Earth-Like Planet', Harvard–Smithsonian Center for Astrophysics; Figure 1.9: ESA; Figure 1.10: NASA/ESA, P. Kalas & J. Graham (UC Berkeley), M. Clampin (NASA/GSFC); Figure 1.11: Marois, C. et al. (2008) 'Direct imaging of multiple planets orbiting the star HR8799', *Science*, **322**, 1348, American Association for the Advancement of Science; Figure 1.14: adapted from Beaugé, C., Ferraz-Mello, S. and Michtchenko, T. A. in *Extrasolar Planets: Formation, Detection and Dynamics*, Dvorak (ed.), Wiley, (2008); Figure 1.15: adapted from Bailey, J. et al. (2009) 'A Jupiter-like planet orbiting the nearby M dwarf GJ 832', *The Astrophysical Journal*, **690**, 743, The American Astronomical Society; Figures 1.16 & 1.17: adapted from Mayor, M. et al. (2004) 'The CORALIE survey for southern-solar planets', *Astronomy and Astrophysics*, **415**, 391, EDP Sciences; Figure 1.18: Photos by David Cortner; Figures 1.19 & 1.20: adapted from Sackett, P. D. (1998) 'Searching for unseen planets via occultation and microlensing', Mariotti, J. and Alloin, D. M. (eds.), 'Planets outside the solar system: theory and observations' (NATO Science series C). Springer; Figure 1.21: Atlas Image obtained as part of the Two Micron All Sky Survey (2MASS), a joint project of the University of Massachusetts and the Infrared Processing and Analysis Center/CalTech, funded by the National Aeronautics and Space Administration and the National Science Foundation, annotations due to K. D. Horne and C. A. Haswell;

Figure 2.1: © University Corporation for Atmospheric Research; Figure 2.2a: Observatoire de Haute Provence; Figure 2.2b: Gdgourou, used under a Creative Commons Attribution-ShareAlike 3.0 Licence; Figure 2.3: adapted from Mazeh, T. et al. (2000), 'The Spectroscopic Orbit of the Planetary Companion transiting HD209458', *The Astrophysical Journal*, **532**, 55, The American Astronomical Society; Figure 2.4: adapted from Charbonneau, D., et al. (2000), 'Detection of planetary transits across a sun-like star', *The Astrophysical Journal*, **529**, 45, The American Astronomical Society; Figure 2.6: © François du Toit; Figure 2.7 adapted from Charbonneau, D., Brown, T. M., Latham, D. W. and Mayor, M. (2000) *The Astrophysical Journal Letters*, **529**, L45; Figure 2.9(a): NASA Jet Propulsion Laboratory (NASA-JPL); Figures 2.10 & 2.11: The SuperWASP Consortium; Figure 2.12(a) adapted from SuperWASP archive by A. J. Norton; Figures 2.12b & 2.20: adapted from Pollacco, D. L., et al. (2006), 'The WASP

Project and the SuperWASP Cameras', *Publications of the Astronomical Society of the Pacific*, **118**, 1407, Astronomical Society of the Pacific; Figure 2.14: adapted from SuperWASP archive by the author; Figure 2.15 adapted from a WASP consortium powerpoint; Figure 2.16: adapted from Collier-Cameron, A., et al. (2007), 'Efficient identification of exoplanetary transit candidates from SuperWASP light curves', *Monthly Notices of the Royal Astronomical Society*, **380**, 1230, The Royal Astronomical Society; Figure 2.17: produced using software written by Rob Hynes; Figure 2.18: adapted from Exoplanet Encyclopedia data by A. J. Norton, A. Dackombe and the author; Figure 2.19: Parley, N. R., (2008) *Serendipitous Asteroid Survey Using SuperWASP*, PhD thesis, The Open University;

Figures 3.1, 3.5 & 3.17: adapted from Brown, T. M. et al. (2001), 'Hubble Space Telescope Time-Series Photometry of the Transiting Planet of HD209458', *The Astrophysical Journal*, **552**, 699, The American Astronomical Society; Figure 3.3: adapted from Sackett, P. D. arXiv:astro-ph/9811269; Figure 3.6: SOHO/ESA/NASA; Figure 3.9a: adapted from Van Hamme, W. (1993), 'New Limb-Darkening Coefficients for modelling Binary Star Light Curves', *The Astronomical Journal*, **106**, Number 5, 2096, The American Astronomical Society; Figure 3.9b: adapted from Morrill J. S. and Korendyke C. M., (2008), 'High-Resolution Center-to-limb variation of the quiet solar spectrum near MgII', *The Astrophysical Journal*, **687**, 646, The American Astronomical Society; Figures 3.10 & 3.11: adapted from Knutson H. A. et al. (2007), 'Using Stellar Limb-Darkening to Refine the Properties of HD 209458 b', *The Astrophysical Journal*, **655**, 564, The American Astronomical Society; Figures 3.16 & 3.18: adapted from Charbonneau, D. et al. (2000), 'Detection of Planetary Transits across a Sun-like Star', *The Astrophysical Journal*, **529**, 45, The American Astronomical Society;

Figures 4.1 & 4.10: adapted from Udry, S. (2008) Extrasolar planets: XVI Canary Islands Winter School of Astrophysics, CUP; Figure 4.2: CNES; Figures 4.3, 4.4, 4.5, 4.6, 4.7 & 4.9: adapted from Exoplanet Encyclopedia data by A. J. Norton, A. Dackombe and the author; Figures 4.8b & c: adapted from Johnson, J. A. (2009), Draft version of submission *International Year of Astronomy Invited Review on Exoplanets*, © John Asher Johnson; Figure 4.11: adapted from Leger, A. et al. (2009), 'Transiting exoplanets from the CoRoT space mission: VIII. CoRoT-7b: the first super-Earth with measured radius', *Astronomy and Astrophysics*, **506**, 287, ESO; Figures 4.12, 4.13 & 4.15: adapted from Guillot, T. (2005) 'The Interiors of Giant Planets: Models and Outstanding Questions', *Annual Review of Earth and Planetary Sciences*, **33**, 493, © Annual Reviews; Figures 4.14 & 4.17: adapted from Liu, X., Burrows, A. and Igbui, L. (2008) 'Theoretical Radii of Extrasolar Giant Planets: the cases of TrES-4, XO-3b and HAT-P-1b', *The Astrophysical Journal*, **687**, 1191, The American Astronomical Society; Figure 4.16: adapted from Arras, P. and Bildsten, L., (2006), 'Thermal Structure and Radius Evolution of Irradiated Gas Giant Planets', *The Astrophysical Journal*, **650**, 394, The American Astronomical Society; Figure 4.19: adapted from Sasselov, D. (2008) 'Astronomy: Extrasolar Planets', *Nature*, **451**, 29; Figure 4.20: adapted from Charbonneau, D. et al. (2006), 'When Extrasolar Planets Transit Their Parent Stars' review chapter in *Protostars and Planets V* (Space Science Series), Jewitt, D. and Reipurth, B. (eds.) University of Arizona Press; Figure 4.21: adapted from Southworth, J. (2008), 'Homogeneous studies of transiting extrasolar planets - I. Light-curve analyses', Monthly Notices of the Royal Astronomical Society, **386**, 1644, The Royal Astronomical Society;

Figure 5.1: adapted from a drawing of Frances Bagenal, University of Colorado; Figure 5.2: adapted from Brown, T. M. (2001) 'Transmission spectra as diagnostics of extrasolar giant planet atmospheres', *The Astrophysical Journal*, **553**, 1006, The American Astronomical Society; Figure 5.4: adapted from Marley, M. S. (2009) 'The atmospheres of extrasolar planets', *Physics and Astrophysics of Planetary Systems*, EDP Sciences; Figure 5.5a: © 2009 Astrobio.net; Figures 5.5b & c and 5.6: adapted from Charbonneau, D. et al. (2002) 'Detection of an extrasolar planet atmosphere', *The Astrophysical Journal*, **568**, 377, The American Astronomical Society; Figure 5.7: adapted from Vidal-Madjar, A. et al. (2003) 'An extended upper atmosphere around the extrasolar planet HD209458b', *Nature*, **422**, 143, Nature Publishing Group; Figure 5.8: adapted from Charbonneau, D. (2003) 'Atmosphere out of that world', *Nature*, **422**, 124, Nature Publishing Group; Figures 5.9 & 5.10a: adapted from Vidal-Madjar, A. et al. (2004) 'Detection of oxygen and carbon in the hydrodynamically escaping atmosphere of the extrasolar planet HD 209458 B', *The Astrophysical Journal*, **604**, 69, The American Astronomical Society; Figure 5.10b: NASA/MSSTA; Figure 5.11: adapted from Sing, D. K. et al. (2009) 'Transit spectrophotometry of the exoplanet HD189733 b. I. Searching for water but finding haze with HST NICMOS', *Astronomy & Astrophysics*, **505**, 819, European Southern Observatory; Figure 5.12: adapted from Désert, J. et al. (2009) 'Search for carbon monoxide in the atmosphere of the transiting exoplanet HD 189733b', *The Astrophysical Journal*, **699**, 478, The American Astronomical Society; Figure 5.13: adapted from Redfield, S. et al. (2008) 'Sodium Absorption from the exoplanetary atmosphere of HD 189733 B detected in the optical transmission spectrum', *The Astrophysical Journal*, **673**, 87, The American Astronomical Society; Figure 5.14: adapted from Scott Gaudi, B. and Winn, J. N. (2007) 'Prospects for the characterization and confirmation of transiting exoplanets via the Rossiter–McLaughlin effect', *The Astrophysical Journal*, **655**, 550, American Astronomical Society; Figures 5.15 & 5.16: adapted from Winn, J. N. (2007) 'Exoplanets and the Rossiter–McLaughlin Effect', *Transiting Extrasolar Planets Workshop*, ASP Conference Series, **336**, 170, Astronomical Society of the Pacific; Figures 5.19a & b: adapted from Triaud, A. H. M. J. et al. (2009) 'The Rossiter–McLaughlin Effect of CoRoT-3b & HD 189733b', *Astronomy and Astrophysics*, **506**, 377, European Space Operations Centre ESOC; Figure 5.19c: adapted from Bouchy, F. et al. (2008) 'Transiting exoplanets from the CoRoT space mission III. The spectroscopic transit of CoRoT-Exo-2b', *Astronomy and Astrophysics*, **482**, 25, European Space Operations Centre; Figures 5.19d & e: adapted from Narita, N. et al. (2009) 'Improved Measurement of the Rossiter–McLaughlin effect in the Exoplanetary System HD 17156', *Publications of the Astronomical Society of Japan*, **61**, 991, Astronomical Society of Japan; Figure 5.19f: adapted from Hébrard, G. et al. (2009) 'Misaligned spin-orbit in the XO-3 planetary system?', *Astronomy and Astrophysics*, **488**, 763, European Southern Observatory; Figure 5.20: adapted from Fabrycky, D. C. and Winn, J. N. (2009) 'Exoplanetary Spin-Orbit Alignment: results from the ensemble of Rossiter–McLaughlin observations', *The Astrophysical Journal*, **696**, 1230, The American Astronomical Society;

Figure 6.1 adapted from Seager, S., Deming, D. and Valenti, J. A. (2008) in *Astrophysics in the Next Decade: The James Webb Space Telescope and Concurrent Facilities*, Thronson, H. A., Stiavelli, M., Tielens, A. (eds.); Figure 6.3: NASA/JPL-Caltech/R. Hurt (SSC); Figure 6.4: adapted from NASA/JPL-Caltech/D. Charbonneau (Harvard–Smithsonian CfA) and NASA/JPL-Caltech/D. Deming (Goddard Space Flight Center); Figure 6.5: adapted from Deming, D. et al. (2006) 'Strong infrared emission from the extrasolar planet HD 189733b', *The Astrophysical Journal*, **644**, 560, The American Astronomical Society; Figure 6.6: adapted from Borucki, W. J. et al. (2009) 'Kepler's optical phase curve of the exoplanet HAT-P-7b', *Science*, **325**, 709, American Association for the Advancement of Science; Figure 6.7: adapted from Charbonneau, D. et al. (2008) 'The broadband infrared emission spectrum of the exoplanet HD 189733b', *The Astrophysical Journal*, **686**, 1341, American Association for the Advancement of Science; Figure 6.8a: adapted from Showman, A. P. et al. (2009) 'Atmospheric circulation of hot jupiters: coupled radiative-dynamical general circulation model simulations of HD189733b and HD209458b', *The Astrophysical Journal*, **699**, 564, The American Astronomical Society; Figure 6.8b: adapted from Knutson, H. A. et al. (2008) 'The 3.6–$8.0\,\mu$m Broadband Emission Spectrum of HD 209458 b: Evidence for an Atmospheric Temperature Inversion' *The Astrophysical Journal*, **673**, 526, IOP Publishing; Figure 6.8c: adapted from Machalek, P. et al. (2008) 'Thermal emission of exoplanet XO-1b', *The Astrophysical Journal*, **684**, 1427, The American Astronomical Society; Figure 6.8d: adapted from Knutson, H. A. et al. (2009) 'Detection of a temperature inversion in the broadband infrared emission spectrum of TrES-4', *The Astrophysical Journal*, **691**, 866, The American Astronomical Society; Figures 6.8e & 6.9: adapted from Machalek, P. et al. (2008) 'Detection of thermal emission of XO-2b: evidence for a weak temperature inversion', *The Astrophysical Journal*, **701**, 514, The American Astronomical Society; Figure 6.10: adapted from Deming, D. (2008) 'Emergent exoplanet flux: review of the Spitzer results', *Transiting Planets — Proceedings of the IAU Symposium*, **253**, 197, International Astronomical Union; Figures 6.11 & 6.12: adapted from Harrington, J. et al. (2006) 'The phase-dependent infrared brightness of the extrasolar planet υ Andromedae b', *Science*, **314**, 623, American Association for the Advancement of Science; Figures 6.13 & 6.14: adapted from Knutson, H. A. et al. (2007) 'A map of the day-night contrast of the extrasolar planet HD 189733b', *Nature*, **447**, 183, Nature Publishing Group;

Figure 7.1: adapted by A. J. Norton from Exoplanet Encyclopaedia; Figure 7.3: adapted from Jones, B. W., Sleep, P. N. and Underwood, D. R. (2006) 'Which exoplanetary systems could harbour habitable planets?', *International Journal of Astrobiology*, **5**(3), 251, CUP; Figure 7.5: NASA/JPL-Caltech/T. Pyle (SSC); Figure 7.6: adapted from Agol, E. et al. (2005) 'On detecting terrestrial planets with timing of giant planet transits', *Monthly Notices of the Royal Astronomical Society*, **359**, 567, The Royal Astronomical Society;

Figure 8.2: adapted from ESA/SRE (2009) PLATO-Next Generation Planet Finder-Assessment Study Report 4, December 2009. ESA; Figure 8.3: MEarth Project; Figure 8.4: adapted from Palle E. et al. (2009) 'Earth's Transmission spectrum from lunar eclipse observations', *Nature*, **459**, 814, Nature Publishing Group; Figures 8.5 & 8.6: adapted from Miller-Ricci, E. and Fortney, J. J. (2010) 'The Nature of the Atmosphere of the Transiting Super-Earth GJ 1214b', *The*

Astrophysical Journal Letters, **716**, L74, The American Astronomical Society; Figure 8.7: adapted from Seager, S., Deming, D. and Valenti, J. A. (2008) ‘Transiting exoplanets with JWST’, Thronson, H. A., Tielens, A., Stiavelli, M., (eds.) *Astrophysics in the Next Decade: JWST and Concurrent Facilities*, 123, Astrophysics & Space Science Library. Springer; Figure 8.8: Lahav, N. (1999) *Biogenesis*, courtesy of Noam Lahav; Figure 8.10: Woods Hole Oceanographic Institute, Deep Submergence Operations Group, Dan Fornari.

Every effort has been made to contact copyright holders. If any have been inadvertently overlooked the publishers will be pleased to make the necessary arrangements at the first opportunity.

Acknowledgements

Grateful acknowledgement is made to the following sources:

Figures

Cover image: An artist's impression of the 'hot Jupiter' exoplanet HD 189733 b transiting across the face of its star (ESA, C. Carreau);

Figure 1: © Lynette R. Cook;

Figure 1.1: NASA Ames Research Center (NASA-ARC); Figures 1.2 and 1.3: Richard Powell, www.atlasoftheuniverse.com, used under a Creative Commons Attribution-ShareAlike 2.5 License; Figure 1.4; generated by the author from RECONs data; Figure 1.5a: adapted from a European Space Agency image; Figure 1.5b: The International Astronomical Union/Martin Kornmesser; Figure 1.5c: Lunar and Planetary Institute/NASA; Figures 1.6a & b and 1.7: NASA Jet Propulsion Laboratory (NASA-JPL); Figure 1.6c: NASA/Goddard Space Center; Figures 1.8 & 8.12: adapted from Kaltenegger, L. (2008) 'Assembling the Puzzle — Evolution of an Earth-Like Planet', Harvard–Smithsonian Center for Astrophysics; Figure 1.9: ESA; Figure 1.10: NASA/ESA, P. Kalas & J. Graham (UC Berkeley), M. Clampin (NASA/GSFC); Figure 1.11: Marois, C. et al. (2008) 'Direct imaging of multiple planets orbiting the star HR8799', *Science*, **322**, 1348, American Association for the Advancement of Science; Figure 1.14: adapted from Beaugé, C., Ferraz-Mello, S. and Michtchenko, T. A. in *Extrasolar Planets: Formation, Detection and Dynamics*, Dvorak (ed.), Wiley, (2008); Figure 1.15: adapted from Bailey, J. et al. (2009) 'A Jupiter-like planet orbiting the nearby M dwarf GJ 832', *The Astrophysical Journal*, **690**, 743, The American Astronomical Society; Figures 1.16 & 1.17: adapted from Mayor, M. et al. (2004) 'The CORALIE survey for southern-solar planets', *Astronomy and Astrophysics*, **415**, 391, EDP Sciences; Figure 1.18: Photos by David Cortner; Figures 1.19 & 1.20: adapted from Sackett, P. D. (1998) 'Searching for unseen planets via occultation and microlensing', Mariotti, J. and Alloin, D. M. (eds.), 'Planets outside the solar system: theory and observations' (NATO Science series C). Springer; Figure 1.21: Atlas Image obtained as part of the Two Micron All Sky Survey (2MASS), a joint project of the University of Massachusetts and the Infrared Processing and Analysis Center/CalTech, funded by the National Aeronautics and Space Administration and the National Science Foundation, annotations due to K. D. Horne and C. A. Haswell;

Figure 2.1: © University Corporation for Atmospheric Research; Figure 2.2a: Observatoire de Haute Provence; Figure 2.2b: Gdgourou, used under a Creative Commons Attribution-ShareAlike 3.0 Licence; Figure 2.3: adapted from Mazeh, T. et al. (2000), 'The Spectroscopic Orbit of the Planetary Companion transiting HD209458', *The Astrophysical Journal*, **532**, 55, The American Astronomical Society; Figure 2.4: adapted from Charbonneau, D., et al. (2000), 'Detection of planetary transits across a sun-like star', *The Astrophysical Journal*, **529**, 45, The American Astronomical Society; Figure 2.6: © François du Toit; Figure 2.7 adapted from Charbonneau, D., Brown, T. M., Latham, D. W. and Mayor, M. (2000) *The Astrophysical Journal Letters*, **529**, L45; Figure 2.9(a): NASA Jet Propulsion Laboratory (NASA-JPL); Figures 2.10 & 2.11: The SuperWASP Consortium; Figure 2.12(a) adapted from SuperWASP archive by A. J. Norton; Figures 2.12b & 2.20: adapted from Pollacco, D. L., et al. (2006), 'The WASP

Project and the SuperWASP Cameras', *Publications of the Astronomical Society of the Pacific*, **118**, 1407, Astronomical Society of the Pacific; Figure 2.14: adapted from SuperWASP archive by the author; Figure 2.15 adapted from a WASP consortium powerpoint; Figure 2.16: adapted from Collier-Cameron, A., et al. (2007), 'Efficient identification of exoplanetary transit candidates from SuperWASP light curves', *Monthly Notices of the Royal Astronomical Society*, **380**, 1230, The Royal Astronomical Society; Figure 2.17: produced using software written by Rob Hynes; Figure 2.18: adapted from Exoplanet Encyclopedia data by A. J. Norton, A. Dackombe and the author; Figure 2.19: Parley, N. R., (2008) *Serendipitous Asteroid Survey Using SuperWASP*, PhD thesis, The Open University;

Figures 3.1, 3.5 & 3.17: adapted from Brown, T. M. et al. (2001), 'Hubble Space Telescope Time-Series Photometry of the Transiting Planet of HD209458', *The Astrophysical Journal*, **552**, 699, The American Astronomical Society; Figure 3.3: adapted from Sackett, P. D. arXiv:astro-ph/9811269; Figure 3.6: SOHO/ESA/NASA; Figure 3.9a: adapted from Van Hamme, W. (1993), 'New Limb-Darkening Coefficients for modelling Binary Star Light Curves', *The Astronomical Journal*, **106**, Number 5, 2096, The American Astronomical Society; Figure 3.9b: adapted from Morrill J. S. and Korendyke C. M., (2008), 'High-Resolution Center-to-limb variation of the quiet solar spectrum near MgII', *The Astrophysical Journal*, **687**, 646, The American Astronomical Society; Figures 3.10 & 3.11: adapted from Knutson H. A. et al. (2007), 'Using Stellar Limb-Darkening to Refine the Properties of HD 209458 b', *The Astrophysical Journal*, **655**, 564, The American Astronomical Society; Figures 3.16 & 3.18: adapted from Charbonneau, D. et al. (2000), 'Detection of Planetary Transits across a Sun-like Star', *The Astrophysical Journal*, **529**, 45, The American Astronomical Society;

Figures 4.1 & 4.10: adapted from Udry, S. (2008) Extrasolar planets: XVI Canary Islands Winter School of Astrophysics, CUP; Figure 4.2: CNES; Figures 4.3, 4.4, 4.5, 4.6, 4.7 & 4.9: adapted from Exoplanet Encyclopedia data by A. J. Norton, A. Dackombe and the author; Figures 4.8b & c: adapted from Johnson, J. A. (2009), Draft version of submission *International Year of Astronomy Invited Review on Exoplanets*, © John Asher Johnson; Figure 4.11: adapted from Leger, A. et al. (2009), 'Transiting exoplanets from the CoRoT space mission: VIII. CoRoT-7b: the first super-Earth with measured radius', *Astronomy and Astrophysics*, **506**, 287, ESO; Figures 4.12, 4.13 & 4.15: adapted from Guillot, T. (2005) 'The Interiors of Giant Planets: Models and Outstanding Questions', *Annual Review of Earth and Planetary Sciences*, **33**, 493, © Annual Reviews; Figures 4.14 & 4.17: adapted from Liu, X., Burrows, A. and Igbui, L. (2008) 'Theoretical Radii of Extrasolar Giant Planets: the cases of TrES-4, XO-3b and HAT-P-1b', *The Astrophysical Journal*, **687**, 1191, The American Astronomical Society; Figure 4.16: adapted from Arras, P. and Bildsten, L., (2006), 'Thermal Structure and Radius Evolution of Irradiated Gas Giant Planets', *The Astrophysical Journal*, **650**, 394, The American Astronomical Society; Figure 4.19: adapted from Sasselov, D. (2008) 'Astronomy: Extrasolar Planets', *Nature*, **451**, 29; Figure 4.20: adapted from Charbonneau, D. et al. (2006), 'When Extrasolar Planets Transit Their Parent Stars' review chapter in *Protostars and Planets V* (Space Science Series), Jewitt, D. and Reipurth, B. (eds.) University of Arizona Press; Figure 4.21: adapted from Southworth, J. (2008), 'Homogeneous studies of transiting extrasolar planets - I. Light-curve analyses', Monthly Notices of the Royal Astronomical Society, **386**, 1644, The Royal Astronomical Society;

Figure 5.1: adapted from a drawing of Frances Bagenal, University of Colorado; Figure 5.2: adapted from Brown, T. M. (2001) 'Transmission spectra as diagnostics of extrasolar giant planet atmospheres', *The Astrophysical Journal*, **553**, 1006, The American Astronomical Society; Figure 5.4: adapted from Marley, M. S. (2009) 'The atmospheres of extrasolar planets', *Physics and Astrophysics of Planetary Systems*, EDP Sciences; Figure 5.5a: © 2009 Astrobio.net; Figures 5.5b & c and 5.6: adapted from Charbonneau, D. et al. (2002) 'Detection of an extrasolar planet atmosphere', *The Astrophysical Journal*, **568**, 377, The American Astronomical Society; Figure 5.7: adapted from Vidal-Madjar, A. et al. (2003) 'An extended upper atmosphere around the extrasolar planet HD209458b', *Nature*, **422**, 143, Nature Publishing Group; Figure 5.8: adapted from Charbonneau, D. (2003) 'Atmosphere out of that world', *Nature*, **422**, 124, Nature Publishing Group; Figures 5.9 & 5.10a: adapted from Vidal-Madjar, A. et al. (2004) 'Detection of oxygen and carbon in the hydrodynamically escaping atmosphere of the extrasolar planet HD 209458 B', *The Astrophysical Journal*, **604**, 69, The American Astronomical Society; Figure 5.10b: NASA/MSSTA; Figure 5.11: adapted from Sing, D. K. et al. (2009) 'Transit spectrophotometry of the exoplanet HD189733 b. I. Searching for water but finding haze with HST NICMOS', *Astronomy & Astrophysics*, **505**, 819, European Southern Observatory; Figure 5.12: adapted from Désert, J. et al. (2009) 'Search for carbon monoxide in the atmosphere of the transiting exoplanet HD 189733b', *The Astrophysical Journal*, **699**, 478, The American Astronomical Society; Figure 5.13: adapted from Redfield, S. et al. (2008) 'Sodium Absorption from the exoplanetary atmosphere of HD 189733 B detected in the optical transmission spectrum', *The Astrophysical Journal*, **673**, 87, The American Astronomical Society; Figure 5.14: adapted from Scott Gaudi, B. and Winn, J. N. (2007) 'Prospects for the characterization and confirmation of transiting exoplanets via the Rossiter–McLaughlin effect', *The Astrophysical Journal*, **655**, 550, American Astronomical Society; Figures 5.15 & 5.16: adapted from Winn, J. N. (2007) 'Exoplanets and the Rossiter–McLaughlin Effect', *Transiting Extrasolar Planets Workshop*, ASP Conference Series, **336**, 170, Astronomical Society of the Pacific; Figures 5.19a & b: adapted from Triaud, A. H. M. J. et al. (2009) 'The Rossiter–McLaughlin Effect of CoRoT-3b & HD 189733b', *Astronomy and Astrophysics*, **506**, 377, European Space Operations Centre ESOC; Figure 5.19c: adapted from Bouchy, F. et al. (2008) 'Transiting exoplanets from the CoRoT space mission III. The spectroscopic transit of CoRoT-Exo-2b', *Astronomy and Astrophysics*, **482**, 25, European Space Operations Centre; Figures 5.19d & e: adapted from Narita, N. et al. (2009) 'Improved Measurement of the Rossiter–McLaughlin effect in the Exoplanetary System HD 17156', *Publications of the Astronomical Society of Japan*, **61**, 991, Astronomical Society of Japan; Figure 5.19f: adapted from Hébrard, G. et al. (2009) 'Misaligned spin-orbit in the XO-3 planetary system?', *Astronomy and Astrophysics*, **488**, 763, European Southern Observatory; Figure 5.20: adapted from Fabrycky, D. C. and Winn, J. N. (2009) 'Exoplanetary Spin-Orbit Alignment: results from the ensemble of Rossiter–McLaughlin observations', *The Astrophysical Journal*, **696**, 1230, The American Astronomical Society;

Figure 6.1 adapted from Seager, S., Deming, D. and Valenti, J. A. (2008) in *Astrophysics in the Next Decade: The James Webb Space Telescope and Concurrent Facilities*, Thronson, H. A., Stiavelli, M., Tielens, A. (eds.); Figure 6.3: NASA/JPL-Caltech/R. Hurt (SSC); Figure 6.4: adapted from NASA/JPL-Caltech/D. Charbonneau (Harvard–Smithsonian CfA) and NASA/JPL-Caltech/D. Deming (Goddard Space Flight Center); Figure 6.5: adapted from Deming, D. et al. (2006) 'Strong infrared emission from the extrasolar planet HD 189733b', *The Astrophysical Journal*, **644**, 560, The American Astronomical Society; Figure 6.6: adapted from Borucki, W. J. et al. (2009) 'Kepler's optical phase curve of the exoplanet HAT-P-7b', *Science*, **325**, 709, American Association for the Advancement of Science; Figure 6.7: adapted from Charbonneau, D. et al. (2008) 'The broadband infrared emission spectrum of the exoplanet HD 189733b', *The Astrophysical Journal*, **686**, 1341, American Association for the Advancement of Science; Figure 6.8a: adapted from Showman, A. P. et al. (2009) 'Atmospheric circulation of hot jupiters: coupled radiative-dynamical general circulation model simulations of HD189733b and HD209458b', *The Astrophysical Journal*, **699**, 564, The American Astronomical Society; Figure 6.8b: adapted from Knutson, H. A. et al. (2008) 'The 3.6–$8.0\,\mu$m Broadband Emission Spectrum of HD 209458 b: Evidence for an Atmospheric Temperature Inversion' *The Astrophysical Journal*, **673**, 526, IOP Publishing; Figure 6.8c: adapted from Machalek, P. et al. (2008) 'Thermal emission of exoplanet XO-1b', *The Astrophysical Journal*, **684**, 1427, The American Astronomical Society; Figure 6.8d: adapted from Knutson, H. A. et al. (2009) 'Detection of a temperature inversion in the broadband infrared emission spectrum of TrES-4', *The Astrophysical Journal*, **691**, 866, The American Astronomical Society; Figures 6.8e & 6.9: adapted from Machalek, P. et al. (2008) 'Detection of thermal emission of XO-2b: evidence for a weak temperature inversion', *The Astrophysical Journal*, **701**, 514, The American Astronomical Society; Figure 6.10: adapted from Deming, D. (2008) 'Emergent exoplanet flux: review of the Spitzer results', *Transiting Planets — Proceedings of the IAU Symposium*, **253**, 197, International Astronomical Union; Figures 6.11 & 6.12: adapted from Harrington, J. et al. (2006) 'The phase-dependent infrared brightness of the extrasolar planet υ Andromedae b', *Science*, **314**, 623, American Association for the Advancement of Science; Figures 6.13 & 6.14: adapted from Knutson, H. A. et al. (2007) 'A map of the day-night contrast of the extrasolar planet HD 189733b', *Nature*, **447**, 183, Nature Publishing Group;

Figure 7.1: adapted by A. J. Norton from Exoplanet Encyclopaedia; Figure 7.3: adapted from Jones, B. W., Sleep, P. N. and Underwood, D. R. (2006) 'Which exoplanetary systems could harbour habitable planets?', *International Journal of Astrobiology*, **5**(3), 251, CUP; Figure 7.5: NASA/JPL-Caltech/T. Pyle (SSC); Figure 7.6: adapted from Agol, E. et al. (2005) 'On detecting terrestrial planets with timing of giant planet transits', *Monthly Notices of the Royal Astronomical Society*, **359**, 567, The Royal Astronomical Society;

Figure 8.2: adapted from ESA/SRE (2009) PLATO-Next Generation Planet Finder-Assessment Study Report 4, December 2009. ESA; Figure 8.3: MEarth Project; Figure 8.4: adapted from Palle E. et al. (2009) 'Earth's Transmission spectrum from lunar eclipse observations', *Nature*, **459**, 814, Nature Publishing Group; Figures 8.5 & 8.6: adapted from Miller-Ricci, E. and Fortney, J. J. (2010) 'The Nature of the Atmosphere of the Transiting Super-Earth GJ 1214b', *The*

Astrophysical Journal Letters, **716**, L74, The American Astronomical Society; Figure 8.7: adapted from Seager, S., Deming, D. and Valenti, J. A. (2008) ‘Transiting exoplanets with JWST’, Thronson, H. A., Tielens, A., Stiavelli, M., (eds.) *Astrophysics in the Next Decade: JWST and Concurrent Facilities*, 123, Astrophysics & Space Science Library. Springer; Figure 8.8: Lahav, N. (1999) *Biogenesis*, courtesy of Noam Lahav; Figure 8.10: Woods Hole Oceanographic Institute, Deep Submergence Operations Group, Dan Fornari.

Every effort has been made to contact copyright holders. If any have been inadvertently overlooked the publishers will be pleased to make the necessary arrangements at the first opportunity.